A 5-step reduced mechanism for combustion of $CO/H_2/H_2O/CH_4/CO_2$ mixtures with low hydrogen/methane and high H_2O content

Z. M. Nicolaou[a], J. Y. Chen[b], N. Swaminathan[a]

[a]*Cambridge University, Department of Engineering, Trumpington Street, Cambridge CB2 1PZ, UK*
[b]*University of California at Berkeley, Department of Mechanical Engineering, 6163 Etcheverry Hall, Mailstop 1740, USA*

Abstract

In this study a 5-step reduced chemical kinetic mechanism involving 9 species is developed for combustion of Blast Furnace Gas (BFG), a multi-component fuel containing $CO/H_2/CH_4/CO_2$, typically with low hydrogen, methane and high water fractions, for conditions relevant for stationary gas-turbine combustion. This reduced mechanism is obtained from a 49-reaction skeletal mechanism which is a modified subset of GRI Mech 3.0. These skeletal and reduced mechanisms are validated for laminar flame speeds, ignition delay times and flame structure with available experimental data, and using computational results with a comprehensive set of elementary reactions. Overall, both the skeletal and reduced mechanisms show a very good agreement over a wide range of pressure, reactant temperature and fuel mixture composition.

Email addresses: `zn209@cam.ac.uk` (Z. M. Nicolaou), `jychen@me.berkeley.edu` (J. Y. Chen), `ns341@cam.ac.uk` (N. Swaminathan)

1. Introduction

Recent developments in gas-turbine power generation include the use of low calorific value fuels. These fuels may be Synthetic Gas which is commonly known as Syngas, Coke Oven Gas (COG) and Blast Furnace Gas (BFG) or suitable combinations of these gases [1]. The constituents of and their relative proportions in these gases vary considerably. The Syngas obtained by coal gasification is mostly composed of hydrogen and carbon monoxide with varying levels of carbon dioxide, water and other trace species [2, 3]. The relative proportions of the predominant gases vary widely depending on the gasification process and the ratio of hydrogen to carbon monoxide mole fractions, $f_{H_2} = X_{H_2}/X_{CO}$, is typically larger than 0.1 and it can be as high as 3 [1, 2, 4, 5, 6, 7, 8]. The industrial COG includes considerable amount of CH_4 in addition to these species with f_{H_2} as high as 11 and $f_{CH_4} \approx 5$ [9], whereas BFG has f_{H_2,CH_4} ranging from 0 to 0.15 [1, 5, 9]. In terms of calorific values, BFG has the lowest value of about 2.95 MJ/m^{3}N compared to 40 MJ/m^{3}N for the standard natural gas used in gas turbines [1].

Robust and accurate models for combustion chemistry and its interaction with turbulence are required for the design and development of gas turbines intend to operate with the above fuels. The combustion chemistry is of particular interest to this study and the turbulence-chemistry interaction will be addressed in future. The wide variation in fuel mixture composition noted above offers a considerable challenge to construct a reliable, robust and computationally efficient chemical kinetic scheme. The computational efficiency is specifically of high importance from the view point of turbulent combustion calculation. Reduced mechanisms offer a convenient way to achieve this

2

objective by reducing number of species involved in the combustion kinetics and yet maintaining an acceptable level of accuracy for important attributes such as laminar burning velocity, flame structure, ignition delays, extinction limits etc. There have been many developments of such reduced mechanisms for the most commonly used single component fuels [10, 11, 12, 13]. Generally, these mechanisms were developed systematically by introducing steady-state and/or partial equilibrium assumptions respectively for some species and reactions involved in a skeletal mechanism. Sensitivity analyses were typically used to obtain a skeletal mechanism from a full comprehensive set of elementary reactions. As noted earlier, these strategies have been used in many past studies to obtain reduced kinetic mechanisms for single component fuels and there has not been an attempt to obtain a reduced mechanism for a multi-species fuel mixture such as the BFG, to the best of the authors' knowledge. Thus, this study makes an attempt in that regard.

The range of validity of a reduced mechanism strongly depends on the fuel composition and operating condition used to develop it. The hydrogen content is low in the BFG as noted earlier and one may like to mix it with small amounts of H_2, CH_4 and H_2O or other gases containing high fractions of these species in order to enhance the BFG combustion characteristics. The need of a reduced mechanism for such multi-species fuels then becomes imperative. Most of the attempts in the past to get reduced mechanisms for a multi-species fuel mixture were for syngas and were validated only for relatively high f_{H_2} values and very low water vapour content [14, 15]. More importantly, the effect of CH_4 was not considered since it was generally taken that the CH_4 content in such fuels was too low to affect the combustion

characteristics which might not be entirely correct. For example, it is later shown in this work that small amounts of CH_4 in a $CO/CH_4/H_2O$-air mixture directly affect the flame speed response to water content in the fuel mixture.

In this study, an accurate reduced kinetic mechanism is developed from a 49-reaction skeletal mechanism which is shown to be suitable for multi-component fuel mixtures containing CO, H_2, H_2O, CO_2 and CH_4, with low f_{H_2} and f_{CH_4} typical for the BFG mixture. This reduced mechanism is then validated for laminar flame speed and its structure, and ignition delay times for pressure and temperature conditions relevant to ground-based heavy weight gas-turbines with typical overall pressure ratios of about 20 or small [3, 5, 16] and combustor inlet temperature not exceeding 1000 K [3, 16]. The reduced mechanism is also assessed for its suitability for high H_2O content in the fuel mixture. To the best of our knowledge this is the first attempt to obtain a reduced mechanism for a multi-component fuel mixture with a good accuracy over a wide range of thermodynamic and thermo-chemical conditions.

The rest of the paper is organised as follows. The skeletal mechanism required for the development of the reduced chemistry is discussed in section 2. The techniques used to develop the reduced mechanism is discussed in section 3 and the reduced mechanism is presented in section 4. The validation results are discussed section 5, its computational advantage is demonstrated in section 6 and the conclusions are summarised in the final section.

2. Development of skeletal mechanism: Sensitivity analysis

The chemical kinetics of CO/H_2 mixture oxidation has been investigated by numerous studies in the past and a sustained interest on the combustion of Syngas in gas turbines for power generation has led to publication of a dedicated volume on this topic in the Combustion Science and Technology journal in 2008. The reviews by Chaos and Dryer [3] and Sung and Law [4] clearly identified the important reactions for CO oxidation are $CO + OH = CO_2 + H$ and $CO + HO_2 = CO_2 + OH$, with the second reactions becoming important at elevated pressures. Comprehensive kinetic mechanisms for dry and moist CO oxidation have been proposed in the past [17, 18] and has been updated in a number of later studies as has been noted by Sung and Law [4]. The interested readers are referred to [4] for further detail.

Out of these many available comprehensive mechanisms, a set of 22-reactions suggested in [15] as a guideline along with the GRI Mech 3.0 is used to obtain a skeletal mechanism in this study. This choice is mainly for the following two reasons. (i) The stiffness of the reduced mechanism, signified by the non-linear coupled equations for steady-state species, strongly depends on the skeletal mechanism used. Wang and Rogg [15] produced a non-stiff and working mechanism for moist CO using their 22 reactions. (ii) The interest in this study also includes the effects of CH_4 on moist CO and thus the GRI Mech 3.0 [19] is used, since this mechanism is widely validated using experimental data for methane [19], H_2O-diluted and oxygen enriched methane [20], moist H_2/CO mixtures at elevated temperature [21] and 323 K [22]. This mechanism was also observed to give reasonable results for flame speeds and ignition delay times for multi-species fuel mixtures over

a wide range of pressure, temperature and fuel composition. Burke et al. [23] noted that the measured mass burning rate of laminar premixed flames of $H_2/CH_4/O_2/He$ mixture of equivalence ratios from 0.3 to 1.0 at pressures from 1 to 25 atmosphere can be obtained using the GRI Mech 3.0, but some of the rate constants need to be adjusted empirically. Kuznetsov et al. [24] concluded that the GRI-3.0 is reasonable to compute the laminar burning velocity of stoichiometric flame of $H_2/O_2/H_2O$ for pressures ranging from 10 to 72 bar but the mechanism of Lutz [25] is better for 1 to 72 bar. The burning velocities calculated by Boushaki et al. [26] for $CH_4/H_2/H_2O/air$ atmospheric flames over a wide range of equivalence ratio with 0-30% H_2, dry (0% H_2O) and wet (100% relative humidity) conditions using the GRI-3.0 compares acceptably well with measurements. He et al. [27] concluded that the laminar flame speeds calculated using the GRI Mech 3.0 and USC-II mechanisms agreed well with their measurements using PLIF techniques for lean flames and USC-II mechanism gives better agreement for flames with equivalence ratio of 0.8 and 0.9. Vasu et al. [28] noted that the GRI-3.0 is able to capture the trends and magnitudes of the measured ignition delays at temperatures 974-1160 K and pressures 1.1-2.6 atmosphere for stoichiometric $H_2/CO/CO_2/air$ mixtures. The analysis of ignition data by Petersen et al. [29] for syngas/air at 600-1148 K and 10-30 atmosphere suggested that the available kinetic mechanisms are reasonable if the temperature is larger than 1000 K, even up to 450 atmosphere as shown in [30]. Two points become clear from this brief survey; the BFG like fuel mixture was not considered in earlier studies and the use of the GRI Mech 3.0 is reasonable as long as the fuel mixture contains molecules such as CO, H_2, CH_4, CO_2 and H_2O.

The mechanism of Wang et al. [15] contains reactions that can also be found in the GRI Mech 3.0 which is very convenient. This is in contrast to the 31-reaction C1/O2 subset of Li et al. [31] for example, where reactions 30 ($HCO + HO_2 = CO_2 + OH + H$) and 31 ($HCO + HCO = H_2 + CO + CO$) do not appear in the GRI set.

In order to identify the most important reactions for fuel mixtures involving both H_2 and CH_4, sensitivity analyses are performed using the GRI [19] reaction set and, its thermodynamic and transport databases. This analysis is discussed next.

2.1. $CO/H_2/H_2O$-air mixtures

In this section, flame speed sensitivity analyses are conducted using the GRI [19], at high (20%) and zero water vapour content in the fuel mixture in order to (1) identify the most important reactions in each case and (2) to obtain a suitable skeletal mechanism for $CO/H_2/H_2O$ mixtures. The skeletal mechanism must be as detailed as possible involving a possibly minimum number of species. This is because the number of species involved is the most important factor affecting the computational time especially in direct numerical simulation (DNS) studies of turbulent combustion. The first 40 most sensitive reactions for $CO/H_2/H_2O$ fuel mixture at an equivalence ratio of $\phi = 0.9$ and reactant temperature of $T_u = 323$ K with $f_{H_2} = 0.053$ and 20% water vapour content are given in Table 1. The sensitivity coefficients are normalised as $S_v^{k_i} = |\frac{k_i}{v}\frac{\partial v}{\partial k_i}|/|\frac{k_i}{v}\frac{\partial v}{\partial k_i}|_{\max}$ where k_i is the specific rate constant for reaction i and v is the flame speed.

Consistent with the findings in [15], the majority of their 22 reactions have the highest sensitivities, but some reactions which are not present in

7

[15] have appeared in Table 1 with higher sensitivities and they must be included. In order of decreasing sensitivity these are reactions 120, 2, 12, 5, 14, and 47. Reactions 35, 36, and 34 do appear in [15] through $H + O_2 + M = HO_2 + M$, but in the GRI there are separate reactions for some of the third body species and should be included. This is also the case for reactions 41, 42 and 40 through $2H + M = H_2 + M$ and reaction 166 through $HCO + M = H + CO + M$. These reactions are shown in bold letters in Table 1. Reactions involving atomic N are neglected since they have low sensitivities in general. Also, note that reactions appearing twice in Table 1 are duplicate reactions (D) in the GRI set.

Considering all of the above changes, 22 from [15], 3 duplicate and 13 additional, a 38-reaction skeletal mechanism is obtained for $CO/H_2/H_2O$-air mixtures with large H_2O percentage.

Further sensitivity analyses were conducted at various conditions. These conditions and the results of this analysis are given in Appendix-A. The following points can be noted from a careful study of the six figures, A1 to A6, shown in this Appendix.

1. When the water vapor is added the sensitivity to the three body recombination reaction $H + O_2 + H_2O = HO_2 + H_2O$ becomes significantly large, while the sensitivity of the corresponding three body reactions involving N_2 and M are reduced. The reaction $H + HO_2 = 2OH$ increases the flame speed being the biggest OH-radical provider as noted in [22]. It is also observed that the sensitivity of the reaction $2OH = O + H_2O$ increases significantly when the moisture content in the fuel mixture is increased thereby increasing OH radical production [21, 22]. This

8

provides an extra source of OH radicals for CO oxidation through the most dominant reaction $OH + CO = H + CO_2$. Also, the sensitivity of chain propagation reaction $OH + H_2 = H + H_2O$ at 20% of water vapour content is reduced. However, as one can see an increase in H_2O concentration shifts the equilibrium of this reaction to the left resulting in more OH which makes fuel mixtures with low H_2 content to be more sensitive to H_2O addition as observed in [21, 22].

2. The chain branching reactions $O + H_2 = H + OH$, $H + O_2 = O + OH$ show increased sensitivities, while the chain carrier reaction $OH + H_2 = H + H_2O$ shows positive sensitivity consistent with the results of [21] when the H_2 fraction in the fuel mixture is increased. Also, the recombination reaction $H + O_2 + H_2O = HO_2 + H_2O$ becomes significant in the dry mixture due to an increased H radical level resulting from the increased H_2 fraction in the mixture. The addition of water vapour in this case does not affect the reaction sensitivities as much for the mixture with low H_2 fraction. This implies that the positive chemical effect of water vapour addition will be less pronounced as observed by Das et al. [22]. The effects are similar to these when the equivalence ratio of the fuel mixture is increased.

3. From a practical point of view in using BFG likes gases, lean mixtures with low H_2 content is of interest. Thus, the effects of reactant temperature and pressure on the reaction sensitivity are also investigated in the Appendix-A. It is well known (see for example [3]) that HO_2 chemistry becomes important at high pressures and thus the CO consuming reaction $HO_2 + CO = OH + CO_2$ has large sensitivities for both dry

and wet mixtures and $OH + CO = H + CO_2$ remains as the most important reaction with sensitivity nearly five times larger than for the HO_2 reaction for CO consumption. As one would expect the sensitivities to the three body recombination reactions are increased at high pressures with $H + O_2 + H_2O = HO_2 + H_2O$ moving up the sensitivity coefficient ranking for wet mixtures as noted for atmospheric conditions. The chain branching reaction $H + O_2 = O + OH$ becomes the second most dominant reaction for both the dry and the wet mixture at high pressures.

Although there is a shift in the ranking of the reactions the more dominant reactions remain the same. Hence it is noted that the reaction make up for the H_2/CO chemistry is unaffected for the range of conditions studied here.

2.2. $CO/CH_4/H_2O$-air mixtures.

The flame speed sensitivity analyses for $CO/CH_4/H_2O$-air mixtures are discussed in this section. This analysis helps one to identify the most important reactions involving CH_4. The normalised flame speed sensitivity coefficients are shown in Table 2 for the first 40 most sensitive reactions from the GRI Mech 3. In this case, the most important reactions involving only CH_4, CH_3 and CH_2O were considered. As a result, in order of decreasing sensitivity, reactions 52, 11, 98, 284, 10, 15, 53, 58, 101 shown in bold letters in Table 2 are added to the 38 reactions identified above. These 9 reactions identified here are also consistent with the study of Cherian et al. [32] although no mechanism was presented in their case for mixtures with high water vapour content, or with CH_4.

10

As for the $CO/H_2/H_2O$ mixtures, additional sensitivity analyses were also conducted for $CO/CH_4/H_2O$ mixture with high and no water vapour. The conditions for this analysis and the raw sensitivity coefficients for the top 20 reactions are shown in Table A1 and Figs. A7 to A12 in the Appendix-A. The following points, in addition to those noted for $CO/H_2/H_2O$ mixtures in section 2.1, can be summarised.

1. It is obvious to expect some reactions involving CH_4, CH_3, CH_2, HCO, CH_2O to show up for CH_4 mixture. More importantly, the chain branching reaction $H + O_2 = O + OH$ moves from 9th rank for $CO/H_2/H_2O$ mixture to 3rd rank for the methane containing mixture and this reaction becomes the most dominant for mixtures with $f_{CH_4} = 1$. This is because of increased level of H resulting from CH_4. Close examination of the net reaction rates of reactions 41-49 (for the methane-containing mixtures), has shown that they are all positive. This means that originally, CH_4 decomposes to CH_3 through reactions 41 and 42. In turn CH_3 decomposes to H through reactions 43 and 44. Thus, addition of methane to a CO mixture results in increased H radical production rate through the above decomposition process. In turn increased H radical production rate causes increased sensitivities of $H + O_2 = O + OH$ and $H + CH_3 + M = CH_4 + M$. The sensitivity of $H + O_2 + H_2O = HO_2 + H_2O$ is also increased (absolute value) as a result, and this explains why CO/CH_4 mixtures are chemically less sensitive to water vapour addition.

2. Another important difference observed is the decrease of the sensitivity of the chain propagation $OH + H_2 = H + H_2O$, moving down from 7th

11

rank to 14th in the top 20 reactions. In the H_2 containing mixtures this reaction can be seen as the fuel attacking step, but for CH_4 containing mixture the fuel attack is signified by reactions involving CH_4 and thus these reactions involving methane take precedence (see Fig. A7). In the wet methane containing mixtures the above chain carrier reaction moves further down in the list.

3. The reaction $O + CH_3 = H + H_2 + CO$ becomes one of the top 7 reactions for dry and wet mixtures with $f_{CH_4} = 1$ at atmospheric pressure. This reaction moves out of the top 20 reactions when the pressure becomes 10 atmosphere.

4. At high pressures (10, 20 atm.), the reaction $O + CH_2O = OH + HCO$ appear in the top 20 reactions but moves out of this set when water vapour is added to the fuel mixture or the pressure is atmospheric.

5. For a relatively high methane concentration in the fuel mixture, reactions with CH_2 and CH_3O become important. For a lower methane content these species are not important for all the conditions tested, hence the reaction make up in the skeletal mechanism is sufficient to describe the methane chemistry of such fuel mixtures. Thus, the effect of small CH_4 amounts in the fuel mixture is adequately captured by the extra 9 reactions noted above, something which was neglected while developing reduced mechanism in a previous study [14].

In order to account for the He, Ar diluted experimental conditions in [33, 34], reactions $H + O_2 + Ar = HO_2 + Ar$ and $H + O_2 + He = HO_2 + He$ are also included in the set assuming that He has the same kinetic parameters as Ar. Slight modifications were made to some of the reaction

rate parameters with respect to their values in the GRI set to improve the agreement with experimental results. These modifications are as follows. (1) The pre-exponential factor of the dominant CO-consuming reaction $OH + CO = H + CO_2$ was reduced by 1.5%, and the pre-exponential factor of the OH-producing reaction $H + HO_2 = 2OH$ was reduced by 1% for better agreement with the experimental data on the flame speeds at high water vapour conditions. (2) The rate of the chain-terminating reaction $H + O_2 + N_2 = HO_2 + N_2$ was reduced by increasing the absolute value of the temperature exponent n by 8% (from n=-1.24 to n=-1.339) and by reducing the pre-exponential factor by 2.5%. This was found to be necessary since the original GRI 3.0 parameters resulted in slight over-estimation of the ignition delay time at low pressure, low temperature conditions. (3) The activation energy of the CO-consuming reaction $HO_2 + CO = OH + CO_2$ was increased by 4%. This was done for better agreement in the high pressure and high temperature regime of the measured ignition delay times since the original GRI 3.0 parameters under-estimated the ignition delay times slightly for these conditions. All the changes made are thus minor and will not de-optimize the set of original GRI Mech 3.0 reactions. These modifications are as per the common practice [23, 35, 36] since they are within the uncertainities of the rate parameters for the above reactions.

Based on the above analysis, the final skeletal mechanism for this study includes 38 reactions suggested in section 2.1, 9 reactions for methane mixtures and 2 three body recombination reaction involving Ar and He identified in this section. Hence, there are 49 reactions involving 15 species in total and this set is given in Table 3 along with the kinetic rate parameters.

3. Development of reduced chemistry

From a numerical standpoint, the time advancement of the species composition corresponds to the solution of a system of stiff ordinary differential equations (ODEs). Without transport phenomena, there are N_s ODEs describing the net rate of change of these species as:

$$\frac{\partial C_i}{\partial t} = \omega_{i,p} - \omega_{i,d}, \quad i = 1...N_s \tag{1}$$

where C_i is the concentration of species i, with a production rate of $\omega_{i,p}$, and a destruction rate of $\omega_{i,d}$. By removing certain intermediate species from the detailed mechanism, the computational effort is reduced as the number of ODEs that must be solved is decreased. For a restricted regime of interest, many intermediate species can be removed from the ODE system without losing the solution accuracy. Intermediate species can be systematically identified and removed from the ODE system via two major sequential steps. First, a skeletal mechanism is generated from the original detailed mechanism using sensitivity analysis as discussed in Section 2. Second, further reduction of the skeletal mechanism results in a reduced mechanism. In the second step, the Quasi-Steady State Assumption (QSSA) (e.g. [11, 37, 38, 39, 40, 41]) can be applied to certain intermediate species. Such a reduced mechanism with QSSA can be described as:

For non-QSS species:

$$\frac{\partial C_i}{\partial t} = \omega_{i,p} - \omega_{i,d}, \quad i = 1...N_{s,reduced} \tag{2a}$$

14

For QSS species:

$$0 = \omega_{j,p} - \omega_{j,d}, \quad j = 1...(N_{s,skeletal} - N_{s,reduced}) \tag{2b}$$

QSSA is applicable to an intermediate species when its production rate, $\omega_{j,p}$ is nearly equal in magnitude to the destruction rate $\omega_{j,d}$ resulting in a very small net change in concentration.

Concentrations of QSS species are solved by the non-linear algebraic system described in Eq. (2b), without any truncation, and identified using a relative error $100(\dot{\omega}_{j,p} - \dot{\omega}_{j,d})/\max(\dot{\omega}_{j,p}, \dot{\omega}_{j,d})$ [42] , whereas non-QSS species concentrations are resolved in the usual manner using Eq. (2a). Computation time saving results from the further decrease in system size from $N_{s,skeletal}$ to $N_{s,reduced}$. Furthermore, the stiffness of the system is also decreased further as species with small life times are removed using a targeted search algorithm (TSA) of Tham et al. [42]. For fast development of reduced chemistry, the interactive Computer Assisted Reduction Mechanism (CARM) algorithm [40, 43] was used for the automatic generation of reduced chemistry with the ability to produce source codes needed for computing the chemical sources. Numerical solutions of the zero-dimensional Perfectly-Stirred Reactor (PSR) with the 49-reaction skeletal mechanism in Table 3 were used as input to CARM.

4. Reduced mechanism

The reduced mechanism is derived from the 49-reaction, 15 species (H, O_2, H_2O, CO, CO_2, H_2, H_2O_2, OH, HO_2, HCO, O, CH_4, CH_3, CH_2O, N_2/He/Ar) skeletal mechanism shown in Table 3. For the He-diluted mixtures the inert

15

N_2 is simply replaced by He along with the different third body efficiencies and the corresponding reaction rate constants. The same would apply in cases where Ar is the inert. During the development, it was found that retaining H_2O_2 instead of HO_2 in the reduced mechanism provides a more robust reduced chemistry. Also, for fine tuning of the reduced chemistry, the activation energy of reaction 2 in Table 3 was increased by 27.5%, a procedure similar to the correction factor employed by Boivin et al. [14] to correctly predict the ignition delay times. This is done because the introduction of steady-state assumptions for some of the species results in over-estimation of their reaction rates. As a result an over-estimation in the reaction rate of the OH radical results in an increased CO consumption rate through the most dominant reaction $CO + OH = CO_2 + H$, leading to an over-estimation of the flame speed. By increasing the activation energy of the chain branching reaction $O + H_2 = H + OH$, the production rates of OH and H radicals are reduced leading to the correct nominal values for the flame speeds. Subsequently, steady-state assumptions are introduced for $HO_2, HCO, CH_3, CH_2O, OH$, and O. The resulting 5-step reduced mechanism involving 9 species is as follows:

$$(1)\ O_2 + H_2O + 3CO => 2H + 3CO_2$$
$$(2)\ CO_2 + H_2 => H_2O + CO$$
$$(3)\ 2H + CO_2 => H_2O + CO$$
$$(4)\ O_2 + 2H_2O + 2CO => 2H + 2CO_2 + H_2O_2$$
$$(5)\ 2H + 4CO_2 + CH_4 => 3H_2O + 5CO$$

The global net rates $\dot{w}_k$ of the non steady-state species involved in the

above 5 steps are then given by:

$$\dot{w}_k = \sum_{j=1}^{Nr} (\nu'' - \nu')_{kj} \dot{w}_{kj}$$

where Nr is the total number of reactions in the skeletal mechanism, ν'' and ν' are the molar stoichiometric coefficients of species k in reaction j on the product and reactant side respectively, and $\dot{w}_{kj}$ is the net rate of species k in reaction j of Table 3. The rate expressions for the 15 species involved in the above 5 steps are given in Appendix-B.

The steady-state relationships include non-linear terms and are solved by point iteration. The steady-state relationships can be written as

$$\frac{dC_A}{dt} = \psi_A(ss, ss') - g_A(ss, ss')C_A = 0,$$

where $\psi_A(ss, ss')$ and $g_A(ss, ss')$ are functions of species both in steady-state, denoted by ss, and non steady-state, denoted by ss'. Here, ψ_A denotes the sum of the rates of reactions producing A and g_A is the sum of the rates of reactions consuming A. The simple point iterative scheme of the following form is used:

$$C_A^{n+1} = \frac{\psi_A(ss, ss')^n}{g_A(ss, ss')^n},$$

where n denotes the iteration number and the iteration procedure is applied sequentially to all steady-state species. The difference $|C_A^{n+1} - C_A^n|$ is monitored and the iteration is considered to be converged for a given species A if $|C_A^{n+1} - C_A^n| \leq A_{\text{tol}}$ where A_{tol} is the tolerance limit defined as $A_{\text{tol}} = \max(C_A \cdot Rel_{\text{tol}}, Abs_{\text{tol}}), Rel_{\text{tol}} = 10^{-5}, Abs_{\text{tol}} = 10^{-15}$. For reduced chemistry with strongly coupled QSS species, a combined point iteration

17

and matrix inversion [44] can be used. Since the current QSS species are not strongly coupled, the point iteration scheme is found to be sufficient for the present case.

5. Validation

Both the skeletal and reduced mechanisms are validated over wide range of conditions shown in Table 4, by comparing laminar flame speeds, ignition delay times and the flame structure with experimental results and/or the computational results obtained using the GRI Mech 3.0 [19]. In the following figures, $f_A = X_A/X_{CO}$ is the ratio of mole fractions of species A to CO. The flame speeds are calculated using the PREMIX [45] code of the CHEMKIN package [46] including the thermal diffusion and multi-component formulation for the species' diffusivities. In the cases where no experimental data are available, the skeletal and the reduced mechanisms are validated against the predictions of the GRI Mech 3.0 [19] and so readers are cautioned while interpreting this particular comparison. In these cases only the mixture-averaged formulation for diffusion is used in order to reduce the computational time for the GRI Mech 3.0 calculations, since a qualitative comparison between the different mechanisms is of interest here, hence the use of multi-component diffusion formulation is less essential.

Ignition delay times are calculated using a constant volume reactor solver of the CHEMKIN package [46]. The ignition delay time was defined as the instant, t_{ign}, corresponding to the maximum temperature gradient with respect to time, $\mathrm{d}T/\mathrm{d}t$. In calculating the ignition delay times with the reduced mechanism, the correction factor used in the study of Boivin et

al. [14] is employed. This correction factor was originally developed in [47] from an analysis of the autoignition eigenvalue under lean conditions. This correction is necessary because the steady-state assumptions for O and OH do not hold during autoignition events leading to under-predictions of the ignition delay times as noted in [14]. The species reaction rates $\dot{W}_k$ are thus corrected by multiplying ($\dot{W}_k^{'} = \dot{W}_k \cdot \Lambda$) with the correction factor Λ given by:

$$\Lambda = \frac{\{(1+2B)^{0.5} - 1\}}{B} \tag{3}$$

where B is given by:

$$B = \frac{2\,k_{f1}C_{O_2}\,(k_{f1}C_{O_2} + k_{f2}C_{H_2} + k_{f3}C_{H_2})}{k_{f2}k_{f3}C_{H_2}^2}. \tag{4}$$

In this study the factor 2, rather than 4 used in [14], in the expression for B is used giving improved agreement with the experimental data. In cases where the steady-states apply such as for example premixed flames, the correction factor is $\Lambda = 1$.

5.1. Premixed flames

Comparisons of computed flame speeds, s_L, against available experimental data for the mixtures listed in Table 4 are presented in Figs. 1-10. The above comparisons show that overall both the skeletal and the reduced mechanism give good agreement with the experimental data and the computations with the GRI Mech 3.0 [19].

Figure 1 presents results for fuel mixtures with $f_{H_2} = 5/95$ and H_2O content up to 36%. Although the experimental data in Fig.1 were not a

19

target of [14], the skeletal mechanism of [14] as implemented in this study, under-predicts the flame speeds for all equivalence ratios and the level of under-prediction increases with the H_2O content in the fuel mixture.

The skeletal mechanism in Table 3 of this work gives good agreement with the experimental results and is slightly more accurate than the mechanism of Li et al. [31] for $\phi = 0.6$. The reduced mechanism also shows a good agreement with the experimental data and captures the increase in flame speed with water content in the fuel. The increase in the flame speed with the addition of water vapor essentially comes from an increase in the OH radical production through the reaction $O + H_2O = 2OH$ identified in section 2 and as suggested in [22]. Consequently, this increases CO consumption rate through the most dominant reaction $CO + OH = CO_2 + H$ as shown by the sensitivity analyses in section 2. Figure 2 compares computational results with the experimental data of [21] for a stoichiometric mixture at 400 K containing low and high hydrogen fractions in the fuel mixture. The agreement is very good for the entire range of water vapour content considered. The inhibiting effect of increased hydrogen fraction in the fuel mixture is clearly seen; for $f_{H_2} = 5/95$ water vapour addition has a net positive chemical effect on the flame speed up to about 15% whereas the water vapour addition yields a monotonic decrease of the flame speed for $f_{H_2} = 1$. As discussed by Singh et al. [21], this is because of the reaction $OH + H_2 = H + H_2O$. For low f_{H_2} the reverse rate is sufficiently large resulting in high total OH production yielding an increased CO consumption rate through $OH + CO = H + CO_2$. This results in a net positive chemical effect on increasing the flame speed. For high f_{H_2}, the forward rate is sufficiently high resulting in OH consumption. This

20

combined with the negative dilution effect of water vapour reduces the flame speed. All of these effects are captured clearly by the reduced mechanism proposed in this study. It is to be noted that updating the heat of formation value for OH from its default value of 9.4 to 8.9 kcal/mol as suggested in [50, 51] yields a maximum over prediction of about 10% for $\phi = 0.9$ case in Fig. 1 when the moisture content is about 18%. This level of over prediction can be reduced by re-optimising the rate parameters for the GRI 3.0 set, which is not the focus of this study. Thus, the default value of 9.4 kcal/mol is used in this study as it gives good agreement for the experimental conditions tested in this study.

Figure 3 compares results with typical syngas mixtures from [27]. The value of f_{CH_4} is kept constant at 0.24 approximately with 11% CO_2 and 42.7% N_2 in the fuel mixture. The skeletal mechanism gives a very good agreement with the experimental results. The reduced mechanism yields a slightly lower values as the hydrogen fraction in the fuel mixture increases but remains within the experimental errors as shown in Fig. 3.

Figure 4 compares the computational results using the skeletal and reduced mechanisms with the experimental results in [48] for CO/H_2-air mixtures. The values of $(X_{CO} + X_{H_2})$ is kept constant while the hydrogen molar fraction, X_{H_2}, in the fuel mixture is varied. For this case, the maximum f_{H_2} value in the fuel is about 0.43. The agreement in Fig. 4 is observed to be good for the entire range of X_{H_2} values considered.

Figure 5 shows the variation of computed flame speeds with equivalence ratio for $CO/H_2/O_2/N_2$ mixtures for reactant temperature ranging from 400 to 700 K. It is to be noted that there is no H_2O vapor in the fuel mixture.

The results are shown for low (top figure) and high (bottom figure) hydrogen fractions in Fig. 5. The experimental data of Natarajan et al. [49] are shown for comparison. The computational results obtained with the 4-step reduced mechanism, and the skeletal mechanism of Boivin et al. [14] as reported in [14] are shown. The skeletal mechanism of [14] as implemented in this study is also shown. The 4-step mechanism [14] over-predicts the flame speed by a large factor for the entire range of equivalence ratio shown in Fig. 5. The flame speeds computed using the skeletal and 5-step reduced mechanisms proposed in this study agree quite well with the experimental measurements for the range of equivalence ratio, reactant temperature and the hydrogen fraction shown in Fig. 5.

Figure 6 shows the computed flame speeds for $CO/H_2/O_2/N_2$ mixture for equivalence ratios larger than in Fig. 5 for $f_{H_2} = 1$. The experimental data shown in Fig. 6 are from the study of Singh et al. [21]. The results in Fig. 6 serve as the additional validation for the mechanisms proposed in this study. At low temperatures the agreement is very good for the entire range of equivalence ratios considered. At higher temperatures the skeletal and reduced mechanisms slightly over-predict the flame speed. This is not surprising since Singh et al. [21] showed that all of the tested mechanisms (GRI Mech 3.0 [19], Davis [52], San Diego [53]) over predicted the flame speed for the range of conditions tested in Fig. 6. The sensitivity analysis by Singh et al. [21] suggested that further studies into the rate constants of the elementary reactions $O + H_2 = H + OH$, $OH + H_2 = H + H_2O$ and $H + O_2 + M = HO_2 + M$ were required. These reactions are expected to be in the top 10 reactions for rich mixture as shown in Fig. A3 in the

22

Appendix-A.

The effect of CO_2 dilution on the flame speed for the Syngas mixture is shown in Fig. 7. The comparisons show that the results computed using the current skeletal and reduced mechanisms are in good agreement with the experimental measurements [49], and these mechanisms capture the CO_2 dilution effects well.

The laminar flame speeds computed using the skeletal and reduced mechanisms at elevated pressures for a range of f_{H_2} values and a wide range of equivalence ratios are compared to the experimental measurements of Sun et al. [33] in Fig. 8. The experimental measurements of Singh et al. [21] at atmospheric pressure are also included in Fig. 8 for further comparison. The agreement observed in this figure is encouraging and indeed very good. Figure 9 compares the variation of mass burning rate with pressure for a rich ($\phi = 2.5$) Ar diluted mixture for $f_{H_2} = 10/90$ measured by Burke et al. [34] to the values computed in this study using the skeletal and reduced mechanisms. The agreement is very good for pressures up to about 5 atm. and for higher pressures in the range of 15-20 atm. There is a slight under prediction of the mass burning rate for 5-15 atm. but it is within the experimental errors as one can see in Fig. 9. In the same study [34] it was shown that there is a maximum in mass burning flux with pressure which is more pronounced as the f_{H_2} ratio increases. However, none of the skeletal mechanisms tested captured this effect satisfactorily, especially in the high pressure regime, and significant deviations were observed between the different mechanisms. In the same study [34] it was concluded that major modifications to the rate parameters may be required for the high pressure regime, as well

as the inclusion of additional reactions. Such a reaction was suggested to be $O + OH + M = HO_2 + M$ which is not included in most skeletal mechanisms.

The flame speeds of some multi-species fuel mixtures from the study of Park et al. [54] are computed and compared in Fig. 10. The highest f_{H_2} value for these cases is 6.0 (bottom figure) and the lowest is 0.55 (top figure), and the corresponding f_{CH_4} values are 3.0 and 0.17 respectively. The middle figure also includes the effect of CO_2 dilution. As one can observe in Fig. 10, both the skeletal and reduced mechanisms show good agreement with the experimental data for all equivalence ratios considered despite the high methane content in the bottom two plots. However, the ratio f_{H_2}/f_{CH_4} is greater than or equal to 2 and thus the H_2 chemical kinetics become more dominant than the methane kinetics. For the mixture with $f_{CH_4} > 1$ however, one observes a slight under prediction of the flame speed for $\phi \geq 0.7$ since extra species such as CH, CH_2, CH_3O, CH_3OH, etc., identified in section 2 (see Table 2) through the sensitivity analyses are required for improved description of the methane chemistry.

The flame speeds computed using the skeletal and reduced mechanism are compared to the results of the GRI mechanism [19] in Fig. 11, since no experimental data are found for this mixture, not only for the pressure and temperature noted in this figure but also for atmospheric conditions. The fuel mixture is composed of CO, H_2, H_2O, CH_4 and CO_2 with $f_{H_2} = 5/95$, $f_{CH_4} = 5/95$ and $f_{CO_2} = 0.5$. It is clear that both the reduced and skeletal mechanism give good agreement even with a high water vapour content in the mixture for both low and high pressures. Figure 12 shows a similar comparison with the same fuel proportions as in Fig. 11 with $f_{CH_4} = 0$ in order to elucidate

24

the effect of CH_4 on the dependence of flame speed on water vapour content. For the case presented in Fig. 11, the methane content is $f_{CH_4} = 5/95$, which is quite small and corresponds to about 2.5% by volume in the fuel mixture. In comparison to Fig. 12 this small addition of CH_4 to the fuel mixture significantly alters the chemical and thermal effect of water vapour. That is, the small amount of CH_4 causes the flame to become chemically less sensitive to water vapour addition since the gradient of s_L with respect to H_2O content is less steep. The reason for this is that less OH radicals are available for CO oxidation through the reaction $OH + CO = H + CO_2$ which is the most important path for CO consumption and the most important reaction as one may see from the sensitivity plots in the Appendix-A. The OH radicals are now directly consumed in the oxidation of CH_4 through $OH + CH_4 = CH_3 + H_2O$ giving more water vapour. This makes the mixture chemically less sensitive to further addition of H_2O, but also thermally more sensitive since H_2O production through the direct oxidation of CH_4 above will increase the product specific heat capacity. All these effects are captured properly by both the reduced and skeletal mechanisms since they include CH_4, in contrast to any existing skeletal or reduced mechanisms for multi-species fuel mixtures.

For the fuel mixture considered in Fig. 13, there is no CH_4 or CO_2. Again there is a good agreement with the full GRI Mech 3.0 [19] and it is some-what improved in the high pressure case, compared to the predictions of the methane-containing fuel mixture in Fig. 11. Figure 14 shows a similar comparison but with no H_2 or CO_2. By comparing Figs. 12 and 13 one can see the effect of CO_2 – the flame speeds are reduced considerably.

The flame structure computed using the skeletal and reduced mechanisms are compared to those from the full GRI Mech 3.0 [19] in Figs. 15-20 over a range of operating conditions including the effects of reactant temperature, pressure and fuel composition. The progress variable, c, in these figures is based on temperature with $c = 0$ denoting the unburnt reactant and $c = 1$ denoting the burnt products. Both the reduced and the skeletal mechanisms show overall good agreement for the major species mass fractions, temperature and heat release rate with the predictions using the GRI Mech 3 [19]. The thermochemical and thermodynamic conditions chosen for Figs. 15 to 20 correspond to those considered for the flame speed comparisons discussed earlier. These results demonstrate the robustness of the skeletal and reduced mechanisms to get the flame structure and it laminar burning velocity over the range of conditions considered in this study.

Although there are no experimental data available for the conditions tested using the GRI Mech 3.0, these comparisons serve to show that (i) the reduced mechanism derived in this study agrees well with the GRI Mech 3.0 results and (ii) the small modifications made to some of the reaction rate parameters as discussed in section 2 do not "de-optimize" the skeletal mechanism.

5.2. Autoignition

Figure 21 compares the computed ignition delay times (with the correction factor in Eq. 3 applied) with the experimental results of Kalitan et al. [55] for CO/H_2 mixtures over a range of conditions listed in Table 4. Overall, the agreement is very good for both low and high pressures and for the entire range of temperatures considered. In the high pressure regime, the values

computed in this study give slightly better agreement for higher temperatures than the skeletal mechanism of Boivin et al. [14] as can be seen for the $f_{H_2} = 20/80$ case at 15.4 atm. Also, one may like to recall that the expression for B in Eq. 4 is modified as noted earlier to yield the agreement shown here and the correction factor is applied over the whole of the integration period.

Figure 22 compares ignition delay times computed for a CO_2-diluted mixture to the measured values in [28] at different pressures. The reduced mechanism shows good agreement with the experimental data for the entire temperature range. The skeletal mechanism also shows a good agreement but seems to slightly over predict the ignition delay times as the pressure is increased. As noted in [28] using sensitivity analysis, the most important reactions at the conditions tested were the chain-branching reactions and the three body recombination reaction $H + O_2 + CO_2 = HO_2 + CO_2$. In the same study it was concluded that the rate of this recombination reaction used in the GRI Mech 3.0 was ideal to be used for kinetic modelling for the temperature range of 800-1305 K and 1-8 atm. Thus, a small reduction in the rate of the chain-branching reactions would certainly improve the agreement for higher pressures but this would only be minor.

Figure 23 shows the computed variation of ignition delay time with mixture temperature for a stoichiometric $CO/H_2/CH_4/H_2O/O_2/N_2$ mixture at 5 atm. The computational results obtained using the skeletal and reduced mechanisms are compared to the experimental data of [56]. It is clear that the reduced mechanism is able to give accurate ignition delay times for such complex multi-species fuel mixture including the effect of water vapour.

6. Speed up times

Table 5 shows the time in seconds taken for each run for each of the conditions shown in Table 4. The flame speeds were calculated using the PREMIX code [45] with thermal diffusion and a multi-component formulation for the species' diffusivities, in a 2.5 cm domain with adaptive grid. It is clear that both the skeletal and reduced mechanisms reduced the computational time significantly compared to the GRI Mech 3.0 [19], while maintaining the same level of accuracy. In particular for case 3 the skeletal mechanism is about 50 times faster and the reduced mechanism about 300 times faster.

7. Conclusions

A 5-step reduced chemical kinetic mechanism involving 9 species for accurate prediction of the combustion characteristics of multi-species fuel mixtures of $CO/H_2/H_2O/CH_4/CO_2$, having low hydrogen/methane and high water vapour content is derived. This mechanism is obtained by applying steady state and partial equilibrium approximations respectively for species and elementary reactions involved in a 49-reaction skeletal mechanism. This skeletal set is obtained from the full GRI Mech 3.0 using sensitivity analysis. These two mechanisms are tested for their ability to predict laminar flame speeds, flame structure and ignition delay times over a wide range of pressure, temperature and fuel mixture composition. The computational results are compared to experimental measurements of the flame speeds available in the literature for a wide range of pressure, 1-20 atm., temperature, 298-700 K and thermo-chemical conditions. The ignition delay times for about $1.1 \leq p \leq 15.4$ atm and $900 \leq T \leq 1320$ K for a range of mixture com-

28

position published in earlier studies are used for validation. The ratio of hydrogen to CO mole fractions varied from 0.05 to 6, methane to CO mole fractions varied from 0.05 to 3 and CO_2 to CO mole fractions varied from 0 to 2.1 for the mixtures tested in this study. These extensive selection of experimental conditions and their comparisons shows a very good agreement over the entire range of conditions considered. It is also worth to note that these conditions are relevant for stationary gas-turbines for power generation. Furthermore, it is found that use of the reduced mechanism decreases the computational time significantly compared to the GRI Mech 3.0, while maintaining a a very good degree of accuracy. To the best of our knowledge, this is the first attempt of a reduced mechanism which can accurately predict the combustion characteristics of such multi-species fuels and with a high water vapour content over a wide range of temperature, pressure and mixture composition. However, experimental data for fuel mixture typical of BFG, containing all of the above species with large amount of CO, equally large amount of CO_2 and small fractions of H_2 and CH_4, is unavailable at this time and experimental investigation of this mixture would be useful.

References

[1] T. Komori, N. Yamagami, H. Hara, Gas Turbine Engineering Section Power Systems Headquarters Mitsubishi Heavy Industries, Ltd. Industrial report (2004). www.mhi.co.jp/power/news/sec1/pdf/2004_nov_04b.pdf. Design for Blast Furnace Gas Firing Gas Turbine.

[2] K. H. Casleton, R. W. Breault, G. A. Richards, Combust. Sci. Technol. 180 (2008) 1013-1056.

[3] M. Chaos, F. L. Dryer, Combust. Sci. Technol. 180 (2008) 1053-1096.

[4] C-.J. Sung, C. K. Law, Combust. Sci. Technol. 180 (2008) 1097-1116.

[5] D. Gielen, Energy Conver. Management. 44 (2003) 1027-1037.

[6] Report: Hydrogen from Coal Program:Research, Development, and Demonstration Plan for the period 2008 through 2016. U.S. Department of Energy (2008).

[7] Report: Wabash River Coal Gasification re-powering Project: A DOE Assesment. U.S. Department of Energy National Energy Technology Laboratory (2002).

[8] O. Maustard, Report: Massachusetts Institute of Technology Laboratory for Energy and the Enviroment (2005). An overview of coal based integrated Gasification Combined Cycle (IGCC) Technology.

[9] O. Gicquel, L. Vervisch, G. Joncquet, B. Labegorre, N. Darabiha, Fuel 82 (2003) 983-991.

[10] A. Patel, S.-C. Kong, R. D. Reitz, ASME 2004-01-0558, 2004.

[11] H. S. Soyhan, P. Amneus, T. Lovas, D. Nilsson, P. Maigaard, F. Mauss, C. Sorusbay, J. Fuels and Lubricants, SAE Transactions 109 (200) 1435-1444.

[12] Y. F. Tham, F. Bisetti, J. Y. Chen, Engineering for Gas Turbines and Power 130 (2008).

[13] H. Wang, M. Frenklach, Combust. Flame 87 (1991) 365-370.

[14] P. Boivin, C. Jimenez, A. L. Sanchez, F. A. Williams. Combust. Flame 158 (2011) 1059-1063.

[15] W. Wang, B. Rogg. Combust. Flame 94 (1993) 271-292.

[16] B. Jones, in: N. Swaminathan and K. N. C. Bray (Eds.), Turbulent Premixed Flames, Cambridge University Press, Cambridge, UK, 2011, pp. 309-351.

[17] R. A. Yetter, F. L. Dryer, H. Rabitz, Combust. Sci. Technol. 79 (1991) 97-2128.

[18] T. J. Kim, R. A. Yetter, F. L. Dryer, Proc. Combust. Inst. 25 (1994) 759-766.

[19] G. P. Smith, D. M. Golden, M. Frenklach, N. W. Moriarty, B. Eiteneer, M. Goldenberg, C. T. Bowman, R. K. Hanson, S. Song, W. C. Gardiner, V. V. Lissianski, Z.Qin, $< http : //www.me.berkeley.edu/gri\_mech >$.

[20] A. N. Mazas, B. Fiorina, D. A. Lacoste, T. Schuller, Combust. Flame 158 (2011) 24282440.

[21] D. Singh, N. Takayuki, T. Saad, L. Qiao, Fuel 94 (2012) 448-456.

[22] A. K. Das, K. Kumar, C. Sung, Combust. Flame 158 (2011) 345-353.

[23] M. P. Burke, F. L. Dryer, Y. Ju, Proc. Combust. Inst. 33 (2011) 905-912.

[24] M. Kuznetsov, R. Redlinger, W. Breitung, J. Grune, A. Friedrich, N. Ichikawa, Proc. Combust. Inst. 33 (2011) 895-903.

[25] A. E. Lutz, A numerical study of thermal ignition. Technical Report SAND88-8228, Sandia National Laboratories, 1988.

[26] T. Boushaki, Y. Dhue, L. Selle, B. Ferret, T. Poinsot, Int. J. Hydr. Energy 37 (2012) 9412-9422.

[27] Y. He, Z. Wanga, L. Yang, R. Whiddon, Z. Li, J. Zhou, K. Chen, 95 (2012) 206-213.

[28] S. S. Vasu, D. F. Davidson, R. K. Hanson, Energy Fuels 25 (2011) 990-997.

[29] E. L. Petersen, D. M. Kalitan, A. B. Barrett, S. C. Reehal, J. D. Mertens, D. J. Beerer, R. L. Hack, V. G. McDonell, Combust. Flame 149 (2007) 244-247.

[30] R. Sivaramakrishnan, A. Comandini, R. S. Tranter, K. Brezinsky, S. G. Davis, H. Wang, Proc. Combust. Inst. 31 (2007) 429-437.

[31] J. Li, Z. Zhao, A. Kazakov, M. Chaos, F. L. Dryer, J.J. Scire Jr., Int. J. Chem. Kin.39 (2007) 109-136.

[32] M.A. Cherian, P. Rhodes, R.J. Simpson, G. Dixon-Lewis, Symp. Int. Combust. 18 (1981) 385-396.

[33] S. Hongyan, S. I. Yang, G. Jomaas, C. K. Law, Proc. Combust. Inst. 31 (2007) 439446.

[34] M. P. Burke, M. Chaos, F. L. Dryer, Y. Ju, Combust. Flame 157 (2010) 618631.

[35] A. K. Das, C.-J. Sung, Y. Zhang, G. Mittal, Int. J. Hydrogen Energy 37 (2012) 6901-6911.

[36] C. L. Rasmussen, J. Hansen, P. Marshall, P. Glarborg, Int. J. Chem. Kin. 40 (2008) 454-480.

[37] T. Turanyi, A. S. Tomlin, M. J. Pilling, J. Phys. Chem. 97 (1993) 163-172.

[38] J. Y. Chen, Transactions of the Aeronautical and Astronautical Society of the Republic of China 33 (2001) 59-67.

[39] J. Warnatz, U. Maas, R. W. Dibble, Combustion 3rd Edition (2001) Springer-Verlag 86-88.

[40] C. J. Montgomery, C. Yang, A. R. Parkinson, J. Y. Chen, Combust. Flame 144 (2006) 37-52.

[41] T. Lovas, D. Nilson, F. Mauss, Symp. Int. Combust. 28 (2000) 1809-1815.

[42] Y.F. Tham, F. Bisetti, J.Y. Chen, Engineering for Gas Turbines and Power 130 (2008).

[43] J. Y. Chen, Workshop on Numerical Aspects of Reduction in Chemical Kinetics, CERMICS-ENPC Cite Descartes-Champus sur Marne, France, September 2, 1997.

[44] J. Y. Chen, Y. F. Tham, Combust. Flame 153 (2008) 634-646.

[45] R.J. Kee, J.F. Grcar, M.D. Smooke, J.A. Miller, Tech. Rep. SAND85-8240 Sandia National Laboratories (1985). A fortran program for modelling steady laminar one-dimensional premixed flames.

[46] R. J. Kee, F. M. Rupley, J. A. Miller, 1992, Chemkin-II: A Fortran Chemical Kinetics Package for the Analysis of Gas Phase Chemical Kinetics, Sandia National Laboratories Report, SAND89-8009B.

[47] P. Boivin, C. Jimenez, A.L. Sanchez, F.A. Williams, Proc. Combust. Inst. (33) 2011 517-523.

[48] C. M. Vagelopoulos, F. N. Egolfopoulos, Symp. Int. Combust. (1994) 1317-1323.

[49] J. Natarajan, T. Lieuwen, J. Seitzman, Combust. Flame 151 (2007) 104-119.

[50] B. Ruscic, A.F. Wagner, L.B. Harding, R.L. Asher, D. Feller, D.A. Dixon, K.A. Peterson, Y. Song, X. Qian, C. Ng, J. Liu, W. Chen, D.W. Schwenke, J. Phys. Chem. A 106, 2002, 2727.

[51] J.T Herbon, R.K. Hanson, D.M. Golden, C.T. Bowman, Proc. Combust. Inst. 29, 2002 1201.

[52] S. G. Davis, A. V. Joshi, H. Wang, F. Egolfopoullos, Proc. Combust. Inst. 30 (2005) 1283-1292.

[53] P. Saxena, F. A. Williams, Combust Flame 145 (2006) 31623.

[54] O. Park, P. S. Veloo, N. Liu, F. N. Egolfopoulos, Proc. Combust. Inst. 33 (2011) 887-894.

[55] D. M. Kalitan, J. D. Mertens, M. W. Crofton, E. L. Petersen, J.Prop.Power 23 (2007) 1291-1303.

[56] E. V. Gurentsov, O. G. Divakov, A. V. Eremin, High Temperature, 40 (2002) 379-386.

$S_v{}^{k_i}$	No. in GRI Mech 3.0 set	Reaction
3.54E-05	209	$NNH + H = H_2 + N_2$
3.76E-05	**40**	$\mathbf{2H + H_2 = 2H_2}$
1.13E-04	208	$NNH + O = NH + NO$
2.21E-04	**42**	$\mathbf{2H + CO_2 = H_2 + CO_2}$
3.30E-04	48	$H + H_2O_2 = OH + H_2O$
3.57E-04	**47**	$\mathbf{H + H_2O_2 = HO_2 + H_2}$
4.33E-04	116(D)	$2HO_2 = O_2 + H_2O_2$
5.68E-04	168	$HCO + O_2 = HO_2 + CO$
6.85E-04	**14**	$\mathbf{O + HCO = H + CO_2}$
7.97E-04	88(D)	$OH + H_2O_2 = HO_2 + H_2O$
8.65E-04	100	$OH + HCO = H_2O + CO$
9.79E-04	1	$2O + M = O_2 + M$
1.12E-03	**5**	$\mathbf{O + H_2O_2 = OH + HO_2}$
1.43E-03	**12**	$\mathbf{O + CO(+M) = CO_2(+M)}$
1.62E-03	89(D)	$OH + H_2O_2 = HO_2 + H_2O$
1.96E-03	**2**	$\mathbf{O + H + M = OH + M}$
2.31E-03	**120**	$\mathbf{HO_2 + CO = OH + CO_2}$
2.33E-03	115(D)	$2HO_2 = O_2 + H_2O_2$
2.40E-03	55	$H + HCO = H_2 + CO$
2.83E-03	**166**	$\mathbf{HCO + H_2O = H + CO + H_2O}$
3.44E-03	**41**	$\mathbf{2H + H_2O = H_2 + H_2O}$
3.64E-03	39	$2H + M = H_2 + M$
5.12E-03	167	$HCO + M = H + CO + M$
8.38E-03	287(D)	$OH + HO_2 = O_2 + H_2O$
1.10E-02	**34**	$\mathbf{H + 2O_2 = HO_2 + O_2}$
1.51E-02	85	$2OH(+M) = H_2O_2(+M)$
1.75E-02	44	$H + HO_2 = O + H_2O$
2.14E-02	4	$O + HO_2 = OH + O_2$
3.36E-02	84	$OH + H_2 = H + H_2O$
5.23E-02	43	$H + OH + M = H_2O + M$
5.96E-02	86	$2OH = O + H_2O$
8.27E-02	33	$H + O_2 + M = HO_2 + M$
9.48E-02	**36**	$\mathbf{H + O_2 + N_2 = HO_2 + N_2}$
9.66E-02	38	$H + O_2 = O + OH$
9.72E-02	87(D)	$OH + HO_2 = O_2 + H_2O$
1.43E-01	3	$O + H_2 = H + OH$
1.69E-01	**35**	$\mathbf{H + O_2 + H_2O = HO_2 + H_2O}$
2.12E-01	45	$H + HO_2 = O_2 + H_2$
3.18E-01	46	$H + HO_2 = 2OH$
1.00E+00	99	$OH + CO = H + CO_2$

Table 1: The first 40 most sensitive reactions from GRI-Mech 3.0. The sensitivity analysis was conducted at T_u=323 K, ϕ=0.9, $f_{H_2} = 5/95$ with H_2O%=20%.

$S_v{}^{k_i}$	No. in GRI Mech 3.0 set	Reaction
2.15E-03	115	$2HO_2 = O_2 + H_2O_2$
2.69E-03	120	$HO_2 + CO = OH + CO_2$
3.07E-03	41	$2H + H_2O = H_2 + H_2O$
3.10E-03	14	$O + HCO = H + CO_2$
3.18E-03	39	$2H + M = H_2 + M$
3.37E-03	168	$HCO + O_2 = HO_2 + CO$
3.39E-03	144	$CH_2(S) + O_2 = H + OH + CO$
3.59E-03	126	$CH + H_2 = H + CH_2$
3.71E-03	100	$OH + HCO = H_2O + CO$
4.16E-03	290	$CH_2 + O_2 => 2H + CO_2$
4.33E-03	95	$OH + CH_3(+M) = CH_3OH(+M)$
5.36E-03	97	$OH + CH_3 = CH_2(S) + H_2O$
5.81E-03	12	$O + CO(+M) = CO_2(+M)$
7.23E-03	**101**	**$OH + CH_2O = HCO + H_2O$**
7.63E-03	**58**	**$H + CH_2O = HCO + H_2$**
7.99E-03	119	$HO_2 + CH_3 = OH + CH_3O$
8.36E-03	44	$H + HO_2 = O + H_2O$
8.91E-03	287	$OH + HO_2 = O_2 + H_2O$
1.01E-02	34	$H + 2O_2 = HO_2 + O_2$
1.10E-02	55	$H + HCO = H_2 + CO$
1.17E-02	84	$OH + H_2 = H + H_2O$
1.42E-02	**53**	**$H + CH_4 = CH_3 + H_2$**
1.59E-02	85	$2OH(+M) = H_2O_2(+M)$
1.59E-02	**15**	**$O + CH_2O = OH + HCO$**
2.09E-02	**10**	**$O + CH_3 = H + CH_2O$**
2.56E-02	**284**	**$O + CH_3 => H + H_2 + CO$**
4.46E-02	86	$2OH = O + H_2O$
4.53E-02	**98**	**$OH + CH_4 = CH_3 + H_2O$**
4.72E-02	**11**	**$O + CH_4 = OH + CH_3$**
4.86E-02	43	$H + OH + M = H_2O + M$
5.50E-02	**52**	**$H + CH_3(+M) = CH_4(+M)$**
7.38E-02	87	$OH + HO_2 = O_2 + H_2O$
7.74E-02	33	$H + O_2 + M = HO_2 + M$
9.20E-02	3	$O + H_2 = H + OH$
9.44E-02	36	$H + O_2 + N_2 = HO_2 + N_2$
1.64E-01	45	$H + HO_2 = O_2 + H_2$
1.73E-01	35	$H + O_2 + H_2O = HO_2 + H_2O$
1.99E-01	38	$H + O_2 = O + OH$
2.50E-01	46	$H + HO_2 = 2OH$
1.00E+00	99	$OH + CO = H + CO_2$

Table 2: The first 40 most sensitive reactions from GRI-Mech 3.0. The sensitivity analysis was conducted at T_u=323 K, ϕ=0.9, $f_{CH_4} = 5/95$ with H_2O%=20%.

	Reaction	A	n	Ea
1	$H + O_2 = O + OH$	2.650E+16	-0.6707	17041.0
2	$O + H_2 = H + OH$	3.870E+04	2.7	6260.0
3	$OH + H_2 = H + H_2O$	2.160E+08	1.51	3430.0
4	$2OH = O + H_2O$	3.570E+04	2.4	-2110.0
5^a	$H + O_2 + M = HO_2 + M$	2.800E+18	-0.86	0.0
6	$H + O_2 + H_2O = HO_2 + H_2O$	1.126E+19	-0.76	0.0
7	$H + O_2 + N_2 = HO_2 + N_2$	2.535E+19	-1.3392	0.0
8	$H + O_2 + He => HO_2 + He$	7.000E+17	-0.8	0.0
9	$H + O_2 + Ar => HO_2 + Ar$	7.000E+17	-0.8	0.0
10	$H + 2O_2 = HO_2 + O_2$	2.080E+19	-1.24	0.0
11	$H + HO_2 = 2OH$	8.316E+13	0	635.0
12	$H + HO_2 = O_2 + H_2$	4.480E+13	0	1068.0
13(D)	$OH + HO_2 = O_2 + H_2O$	1.450E+13	0	-500.0
14(D)	$OH + HO_2 = O_2 + H_2O$	5.000E+15	0	17330.0
15	$H + HO_2 = O + H_2O$	3.970E+12	0	671.0
16	$O + HO_2 = OH + O_2$	2.000E+13	0	0.0
17(D)	$2HO_2 = O_2 + H_2O_2$	1.300E+11	0	-1630.0
18(D)	$2HO_2 = O_2 + H_2O_2$	4.200E+14	0	12000.0
19^b	$2OH(+M) = H_2O_2(+M)$	7.400E+13	-0.37	0.0
20	$H + H_2O_2 = OH + H_2O$	1.000E+13	0	3600.0
21(D)	$OH + H_2O_2 = HO_2 + H_2O$	1.700E+18	0	29410.0
22(D)	$OH + H_2O_2 = HO_2 + H_2O$	2.000E+12	0	427.0
23	$H + H_2O_2 = HO_2 + H_2$	1.210E+07	2	5200.0
24	$O + H_2O_2 = OH + HO_2$	9.630E+06	2	4000.0
25^c	$2H + M = H_2 + M$	1.000E+18	-1	0.0
26	$2H + H_2 = 2H_2$	9.000E+16	-0.6	0.0
27	$2H + CO_2 = H_2 + CO_2$	5.500E+20	-2	0.0
28	$2H + H_2O = H_2 + H_2O$	6.000E+19	-1.25	0.0
29^d	$H + OH + M = H_2O + M$	2.200E+22	-2	0.0
30^e	$2O + M = O_2 + M$	1.200E+17	-1	0.0
31^f	$O + H + M = OH + M$	5.000E+17	-1	0.0
32	$OH + CO = H + CO_2$	4.689E+07	1.228	70.0
33	$HO_2 + CO = OH + CO_2$	1.500E+14	0	24544.0
34^g	$O + CO(+M) = CO_2(+M)$	1.800E+10	0	2385.0
35	$H + HCO = H_2 + CO$	7.340E+13	0	0.0
36	$OH + HCO = H_2O + CO$	5.000E+13	0	0.0
37	$HCO + O_2 = HO_2 + CO$	1.345E+13	0	400.0
38^h	$HCO + M = H + CO + M$	1.870E+17	-1	17000.0
39	$HCO + H_2O = H + CO + H_2O$	1.500E+18	-1	17000.0
40	$O + HCO = H + CO_2$	3.000E+13	0	0.0
41	$O + CH_4 = OH + CH_3$	1.020E+09	1.5	8600.0
42	$OH + CH_4 = CH_3 + H_2O$	1.000E+08	1.6	3120.0
43	$O + CH_3 = H + CH_2O$	5.060E+13	0	0.0
44	$O + CH_3 => H + H_2 + CO$	3.370E+13	0	0.0
45	$O + CH_2O = OH + HCO$	3.900E+13	0	3540.0
46^i	$H + CH_3(+M) = CH_4(+M)$	1.390E+16	-0.534	536.0
47	$H + CH_4 = CH_3 + H_2$	6.600E+08	1.62	10840.0
48	$H + CH_2O = HCO + H_2$	5.740E+07	1.9	2742.0
49	$OH + CH_2O = HCO + H_2O$	3.430E+09	1.18	-447.0

Table 3: The skeletal mechanism. Units are in cm, s, mol, cal, K.

[a]: O_2/0.0, H_2O/0.0, CO/0.75, CO_2/1.5, N_2/0.0, Ar/0.0, He/0.0

[b]: Low:2.300E+18/-0.900/-1700.00, Troe: 0.7346/94.00/1756.00/5182.00, H_2/2.0, H_2O/6.0, CH_4/2.0, CO/1.5, CO_2/2.0, Ar/0.7, He/0.7

[c] H_2/0.0, H_2O/0.0, CH_4/2.0, CO_2/0.0, Ar/0.63, He/0.63

[d] H_2/0.73, H_2O/3.65, CH_4/2.0,Ar/0.38, He/0.38

[e]: H_2/2.4, H_2O/15.4, CH_4/2.0, CO/1.75, CO_2/3.6, Ar/0.83, He/0.83

[f] H_2/2.0, H_2O/6.0, CH_4/2.0, CO/1.5, CO_2/2.0, Ar/0.7, He/0.7

[g]: Low: 6.020E+14/0.0/3000.00, H_2/2.0, O_2/6.0, H_2O/6.0, CH_4/2.0, CO/1.5, CO_2/3.5, Ar/0.5, He/0.5

[h]: H_2/2.0, H_2O/0.0, CH_4/2.0, CO/1.5, CO_2/2.O

[i]: Low: 2.620E+33/-4.760/2440.00, Troe: 7830.0/74.00/2941.00/6964.00, H_2/2.0, H_2O/6.0, CH_4/3.0, CO/1.5, CO_2/2.0, Ar/0.7, He/0.7

Fuel	Oxidizer	$f_{H_2} = X_{H_2}/X_{CO}$	f_{CH_4}	f_{CO_2}	$H_2O\%$	p(atm)	T_u(K)	ϕ	Comparison
Flame speed:									
$CO/H_2/H_2O$[1]	Air	5/95	0	0	0-36	1	323	0.6-0.9	[?], Fig.1
$CO/H_2/H_2O$[1]	Air	5/95	0	0	0-40	1	400	0.6-0.9	[21], Fig.2
$CO/H_2/CH_4/CO_2/N_2$	Air	Vary	0.24	11%	0	1	298	1.0,0.9,0.8	[27], Fig.3
CO/H_2	Air	Vary	0	0	0	1	303	-	[48], Fig.4
CO/H_2	Air	5/95	0	0	0	1	400-700	0.2-1.1	[49], Fig.5
CO/H_2	Air	1	0	0	0	1	400-700	0.2-1.1	[49], Fig.5
CO/H_2	Air	1	0	0	0	1	298-500	0.7-3.0	[21], Fig.6
$CO/H_2/CO_2$	Air	5/95	0	0.117	0	1	298	0.5-1.2	Fig.7
$CO/H_2/CO_2$	Air	1	0	0.5	0	1	298	0.5-1.2	[49], Fig.7
CO/H_2	Air	5/95	0	0	0	1	298	0.5-1.2	[49], Fig.7
CO/H_2	Air	1	0	0	0	1	298	0.5-1.2	[49], Fig.7
CO/H_2	Air	1/99	0	0	0	1	298	0.5-5.0	[33], Fig.8
CO/H_2	Air	5/95	0	0	0	1	298	0.5-5.0	[33], Fig.8
CO/H_2	Air	25/75	0	0	0	1	298	0.5-5.0	[33], Fig.8
CO/H_2	Air	50/50	0	0	0	1	298	0.5-5.0	[33], Fig.8
CO/H_2	Air	75/25	0	0	0	1	298	0.5-5.0	[21], Fig.8
CO/H_2[2]	O_2/He	10/30	0	0	0	5,10,20	298	0.5-5.0	[33], Fig.8
CO/H_2	O_2/He	1	0	0	0	5,10	298	0.5-5.0	[33], Fig.8
CO/H_2	O_2/Ar	10/90	0	0	0	1-20	295	2.5	[34], Fig.9
$CO/H_2/CH_4$	Air	0.55	0.17	0	0	1	298	0.4-1.2	[54], Fig.10
$CO/H_2/CH_4$	Air	6	3	0	0	1	298	0.4-1.2	[54], Fig.10
$CO/H_2/CH_4/CO_2$[3]	Air	4.9	2.27	0.91	0	1	298	0.5-1.2	[54], Fig.10
$CO/H_2/CH_4/H_2O/CO_2$	Air	5/95	5/95	0.5	0-70	1,10	600	0.7,1.0	[19], Fig.11
$CO/H_2/H_2O/CO_2$	Air	5/95	0	0.5	0-70	1,10	600	0.7,1.0	[19], Fig.12
$CO/H_2/H_2O$	Air	5/95	0	0	0-70	1,10	600	0.7,1.0	[19], Fig.13
$CO/CH_4/H_2O$	Air	0	5/95	0	0-70	1,10	600	0.7,1.0	[19], Fig.14
Flame structure:									
CO/H_2	Air	5/95	0	0	0	1	400	0.8	[19], Fig.15
CO/H_2	Air	5/95	0	0	0	1	700	0.8	[19], Fig.16
CO/H_2	O_2/He	1	0	0	0	5	298	2	[19], Fig.17
CO/H_2	O_2/He	1	0	0	0	10	298	2	[19], Fig.18
$CO/H_2/CH_4/CO_2/H_2O$	Air	5/95	5/95	0.5	25	1	600	1	[19], Fig.19
$CO/H_2/CH_4/CO_2/H_2O$	Air	5/95	5/95	0.5	25	10	600	1	[19], Fig.20
Ignition delay times:									
CO/H_2	Air	4	0	0	0	1.1	900-1340	0.5	[55], Fig.21
CO/H_2	Air	1.5	0	0	0	1.1	900-1340	0.5	[55], Fig.21
CO/H_2	Air	0.67	0	0	0	1.1	900-1340	0.5	[55], Fig.21
CO/H_2	Air	0.25	0	0	0	1.2,15.4	900-1340	0.5	[55], Fig.21
CO/H_2[4]	Air	0.11	0	0	0	1.1,14.9	900-1340	0.5	[55], Fig.21
$CO/H_2/CO_2$	Air	0.77	0	2.1	0	1.24-2.36	900-1340	1.0	[28], Fig.22
$CO/H_2/H_2O/CH_4$	Air	3	1	0	10%	5	1017-1197	1.0	[28], Fig.23

Table 4: The range of fuel composition and operating conditions tested.

Case (sl)	Conditions	GRI Mech 3.0	49r-skeletal	5-step
1	H2O%=20, ϕ=0.9	1415.099	47.559	5.941
2	p=20atm, ϕ=5.0	7956.458	284.573	29.179
3	ϕ=1.2	2903.111	51.992	9.044

Table 5: Time in s of the run for each condition using PREMIX [45] with thermal and multi-component diffusion.
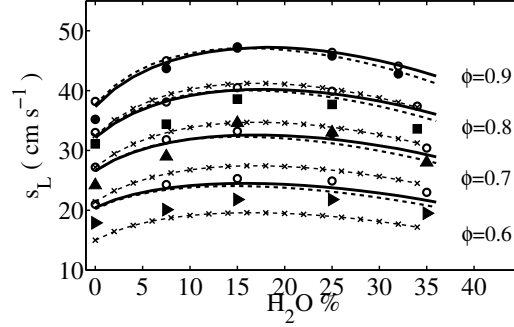
Fig. 1: Laminar flame speeds of $CO/H_2/H_2O$-air mixtures using the reduced (dashed lines) and skeletal (full lines) mechanisms. Open circles: Li et al. [31] mechanism results from [22]. Also shown are the predictions using the skeletal mechanism of Boivin et al. (dashed lines with $\times$) [14]. Filled symbols: experimental results of Das et al. [22]. $T_u = 323$ K, $p = 1$ atm, $f_{H_2} = 5/95$, $X_{N_2}/X_{O_2} = 3.76$.
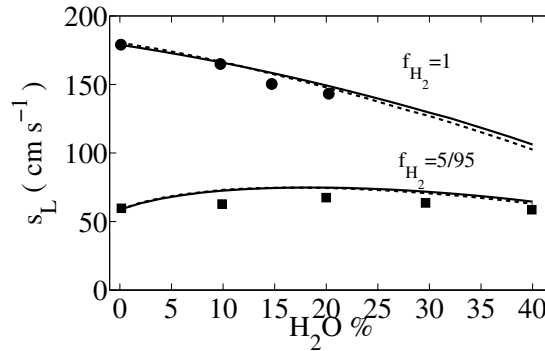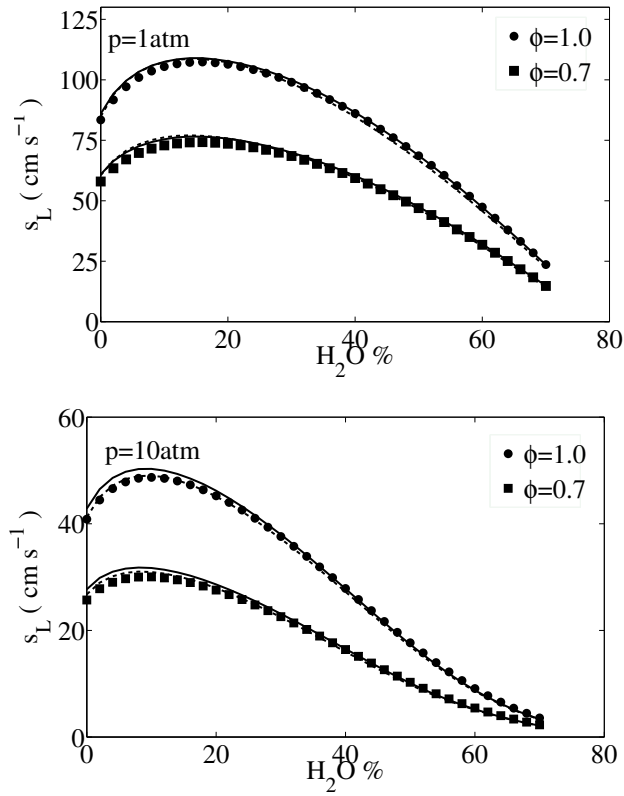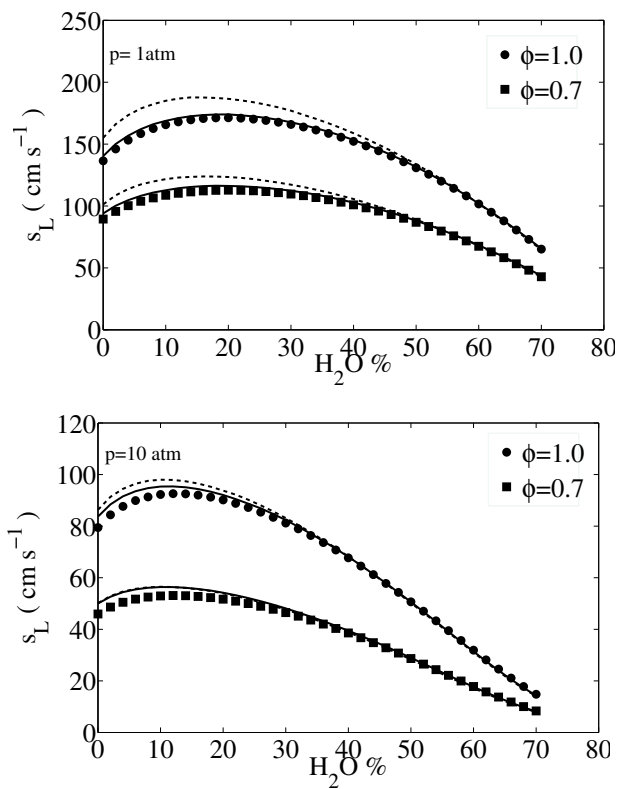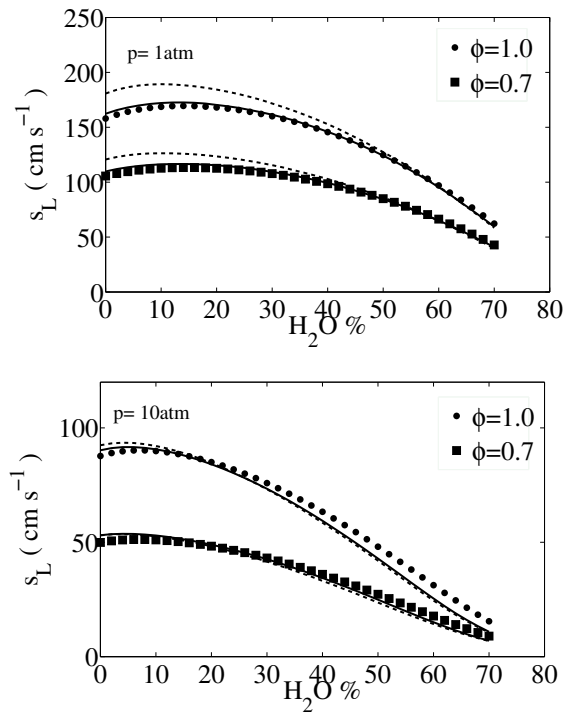

Fig. 2: Laminar flame speeds of $CO/H_2/H_2O$ mixtures using the reduced (dashed lines) and skeletal (continuous lines) mechanisms. Filled symbols: experimental results of Singh et al. [21]. $p = 1$ atm, $T_u = 400$ K, $\phi = 1$, oxidiser is O_2, N_2 with $X_{N_2}/X_{O_2} = 3.76$.

42
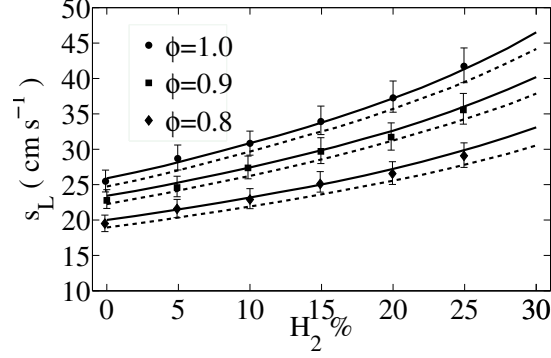
Fig. 3: Laminar flame speeds of syngas mixtures ($CO/H_2/CH_4/CO_2/N_2$-air) using the reduced (dashed lines) and the skeletal (full lines) mechanisms. Symbols: experimental results of Yong et al. [27]. $f_{CH_4} = 0.24$ with 11% CO_2 and 42.7% N_2 in the fuel mixture. $T_u = 298$ K, $p = 1$ atm, $X_{N_2}/X_{O_2} = 3.76$. Error bars from [27] are also shown.
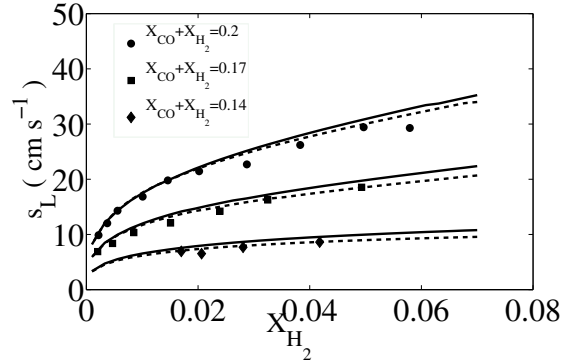
Fig. 4: Laminar flame speeds of CO/H_2-air mixtures using the reduced (dashed lines) and skeletal (full lines) mechanisms. Symbols: experimental results of Vagelopoulos and Egolfopoulos [48]. $T_u = 298$ K, $p = 1$ atm, $X_{N_2}/X_{O_2} = 3.76$.
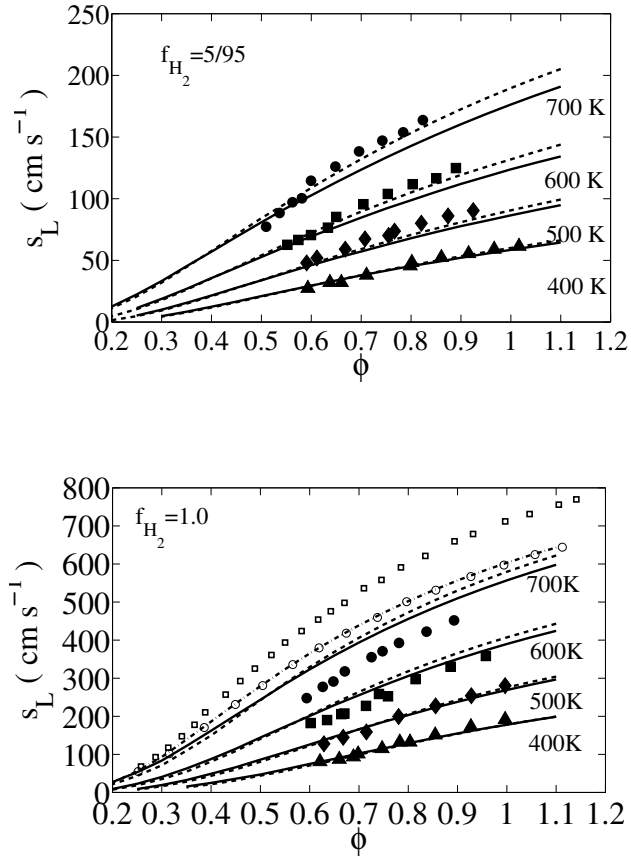
Fig. 5: Laminar flame speeds of $CO/H_2/O_2/N_2$ mixtures using the reduced (dashed lines) and skeletal (continuous lines) mechanisms. Also shown are the results using the 4-step reduced mechanism of [14] (open squares), the skeletal mechanism of [14] (open circles) from the same study, and the implementation of the skeletal mechanism of [14] in this study (dashed-dotted lines). Symbols: experimental results of Natarajan et al. [49]. $f_{H_2} = 5/95$ and 1.0, at $p = 1$ atm, $X_{N_2}/X_{O_2} = 3.76$, for $T_u = 400$, 500, 600 and 700 K.
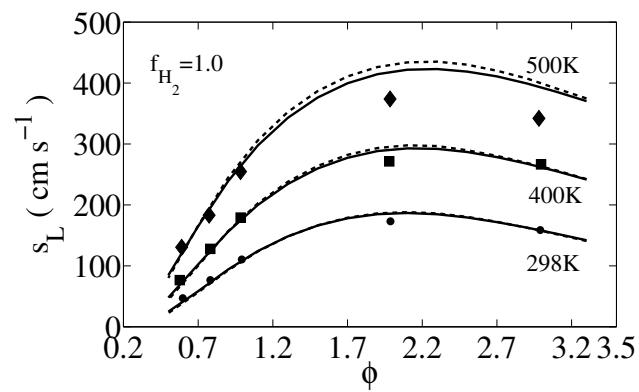
Fig. 6: Laminar flame speeds of CO/H$_2$ mixtures using the reduced (dashed lines) and skeletal (continuous lines) mechanisms. Filled symbols: experimental results of Singh et al. [21]. $p = 1$ atm, oxidizer is air.
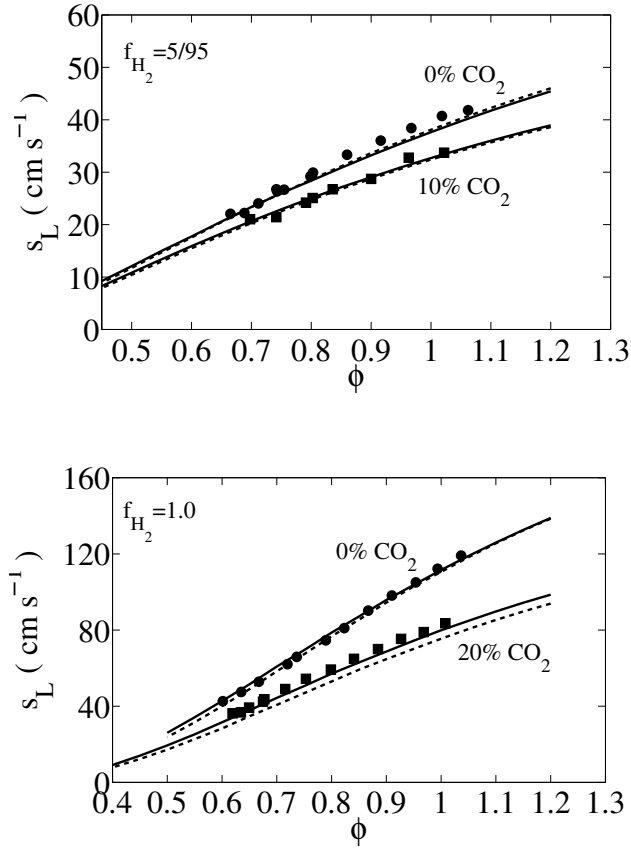
Fig. 7: Laminar flame speeds of $CO/H_2/CO_2/O_2/N_2$ mixtures using the reduced (dashed lines) and skeletal (continuous lines) mechanisms . Symbols: experimental results of Natarajan et al. [49]. $f_{H_2} = 5/95$ and 1.0, at $p = 1$ atm, $X_{N_2}/X_{O_2} = 3.76$ with 10% and 20% CO_2 dilution.
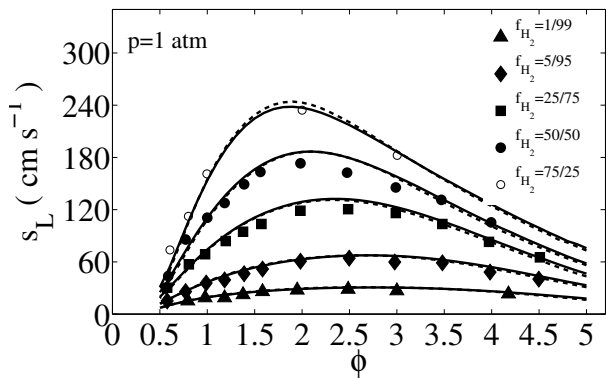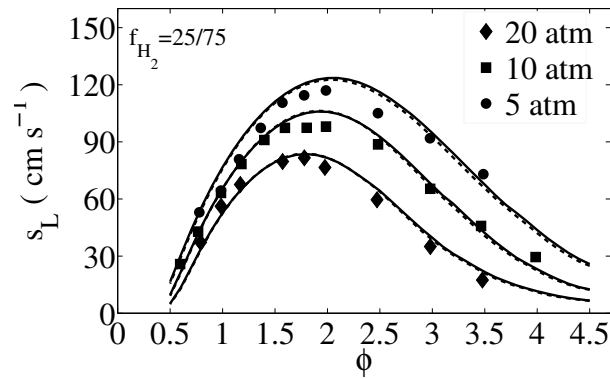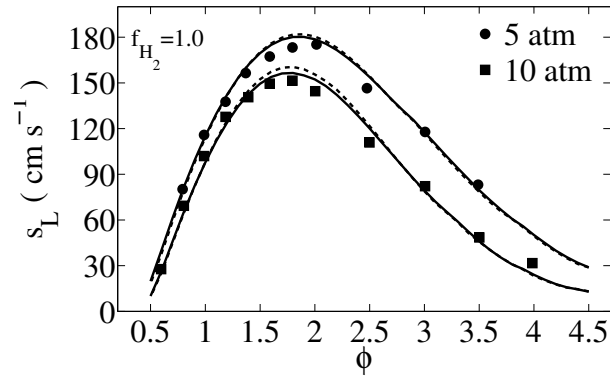
Fig. 8: Laminar flame speeds of CO/H$_2$ mixtures using the reduced (dashed lines) and skeletal (continuous lines) mechanisms. Symbols: experimental results of Sun et al. [33]. At $p = 1$ atm the oxidizer is O$_2$, N$_2$ with $X_{N_2}/X_{O_2} = 3.76$. At $p = 5, 10, 20$ atm the oxidizer is O$_2$ and He with $X_{He}/X_{O_2} = 7.0$. Open symbols: experimental results of Singh et al. [21].

47
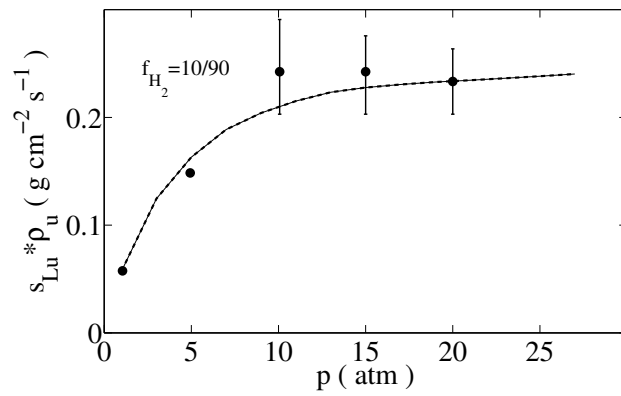
Fig. 9: Laminar flame mass burning rate for $CO/H_2/O_2/Ar$ mixtures using the reduced (dashed lines) and skeletal (continuous lines) mechanisms. Filled symbols: experimental data of Burke et al. [34]. $T_u = 295$ K, $\phi = 2.5$, $X_{Ar}/X_{O_2} = 10.95$.
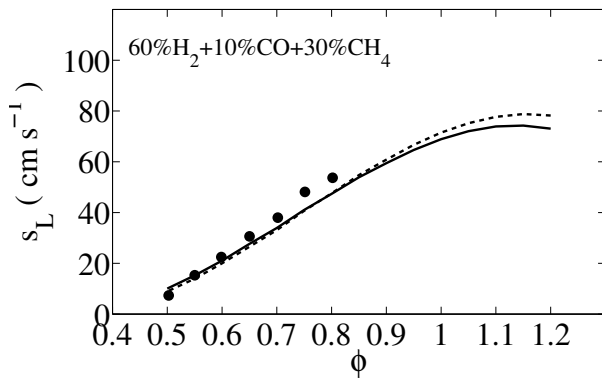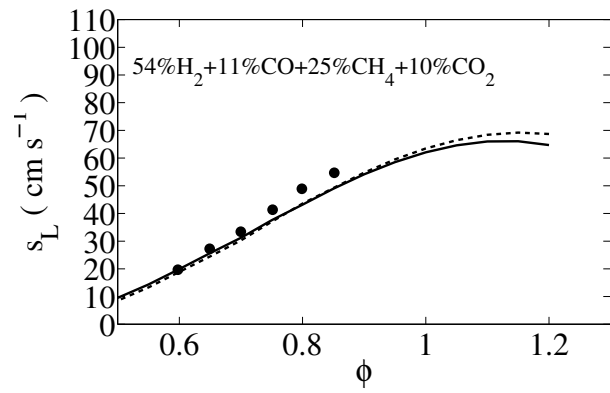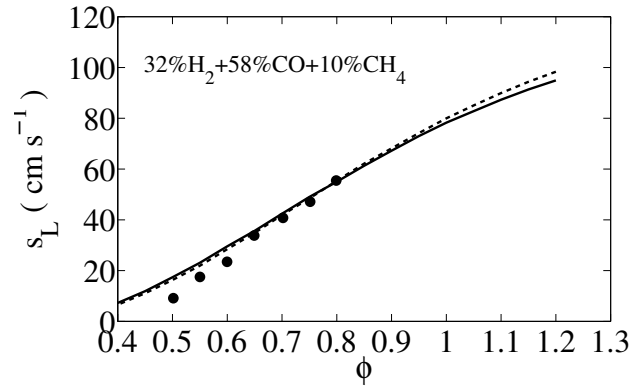
Fig. 10: Laminar flame speeds of $CO/H_2/CH_4/CO_2/O_2/N_2$ mixtures using the reduced (dashed lines) and skeletal (continuous lines) mechanisms. Symbols: experimental results of Park et al. [54], $p = 1$ atm, $T_u = 298$ K. 49
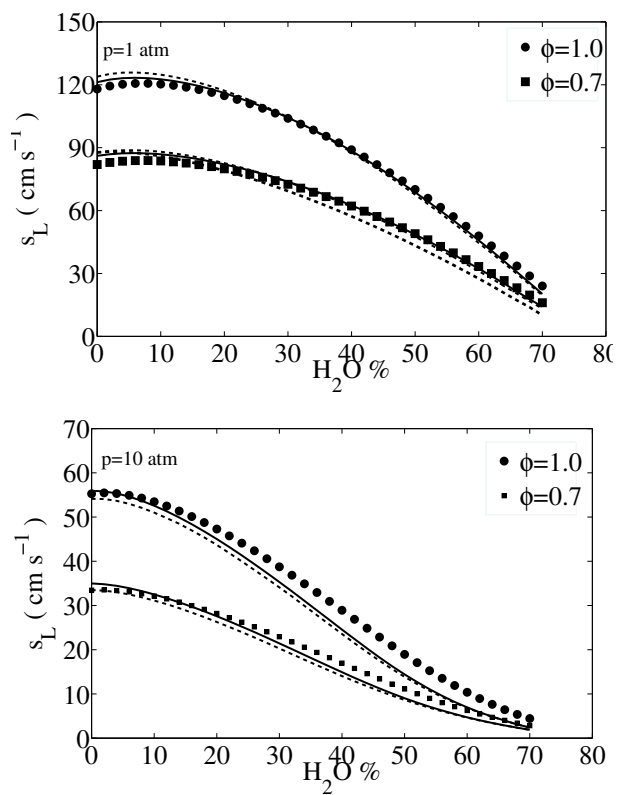
Fig. 11: Laminar flame speeds of $CO/H_2/CH_4/H_2O/CO_2/O_2/N_2$ mixtures using the reduced (dashed lines) and skeletal (continuous lines) mechanisms. Symbols: GRI Mech 3.0 results. $f_{H_2} = 5/95$, $f_{CH_4} = 5/95$, $f_{CO_2} = 0.5$, $T_u = 600$ K at $p = 1$ and 10 atm.

Fig. 12: Laminar flame speeds of $CO/H_2/H_2O/CO_2/O_2/N_2$ mixtures using the reduced (dashed lines) and skeletal (continuous lines) mechanisms. Symbols: GRI Mech 3.0 results. $f_{H_2} = 5/95$, $f_{CO_2} = 0.5$, $T_u = 600$ K at $p = 1$ and 10 atm.

Fig. 13: Laminar flame speeds of $CO/H_2/H_2O/O_2/N_2$ mixtures using the reduced (dashed lines) and skeletal (continuous lines) mechanisms. Symbols: GRI Mech 3.0 predictions. $f_{H_2} = 5/95$, $T_u = 600$ K at $p = 1$ and 10 atm.

Fig. 14: Laminar flame speeds of $CO/CH_4/H_2O/O_2/N_2$ mixtures using the reduced (dashed lines) and skeletal (continuous lines) mechanisms. Symbols: GRI Mech 3.0 predictions. $f_{CH_4} = 5/95$, $T_u = 600$ K at $p = 1$ and 10 atm.
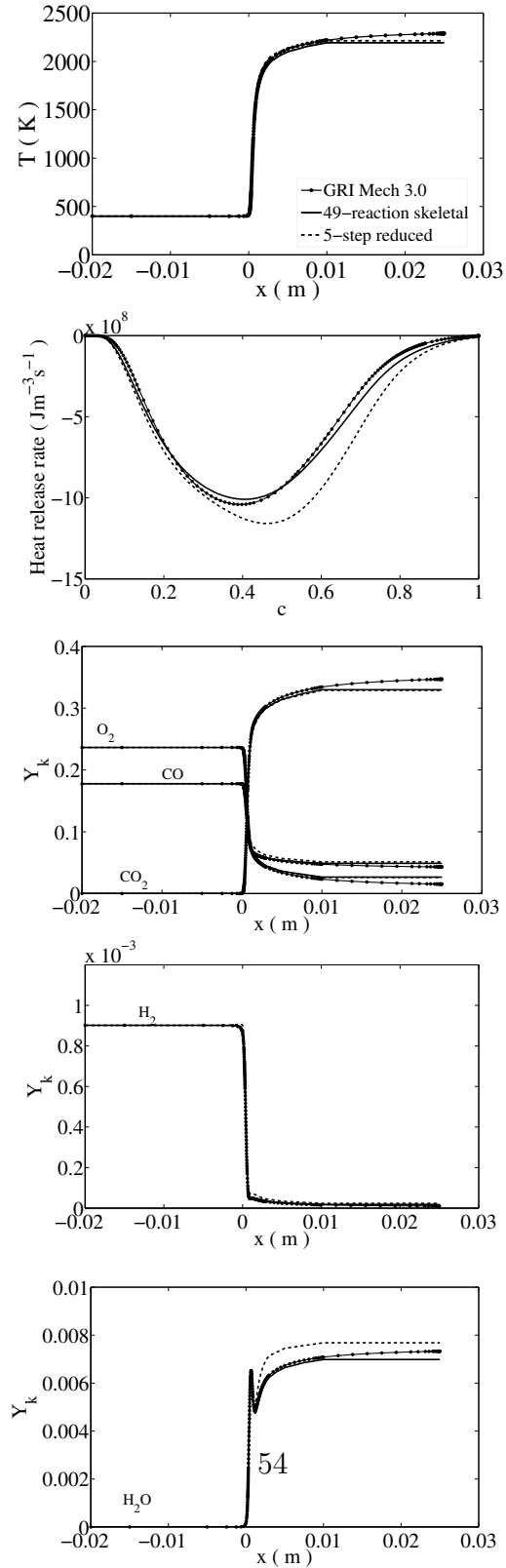
Fig. 15: Flame structure for $CO/H_2/O_2/N_2$. $\phi = 0.8$, $f_{H_2} = 5/95$, $T_u = 400$ K, $p = 1$ atm. (conditions as in Fig.5 top).
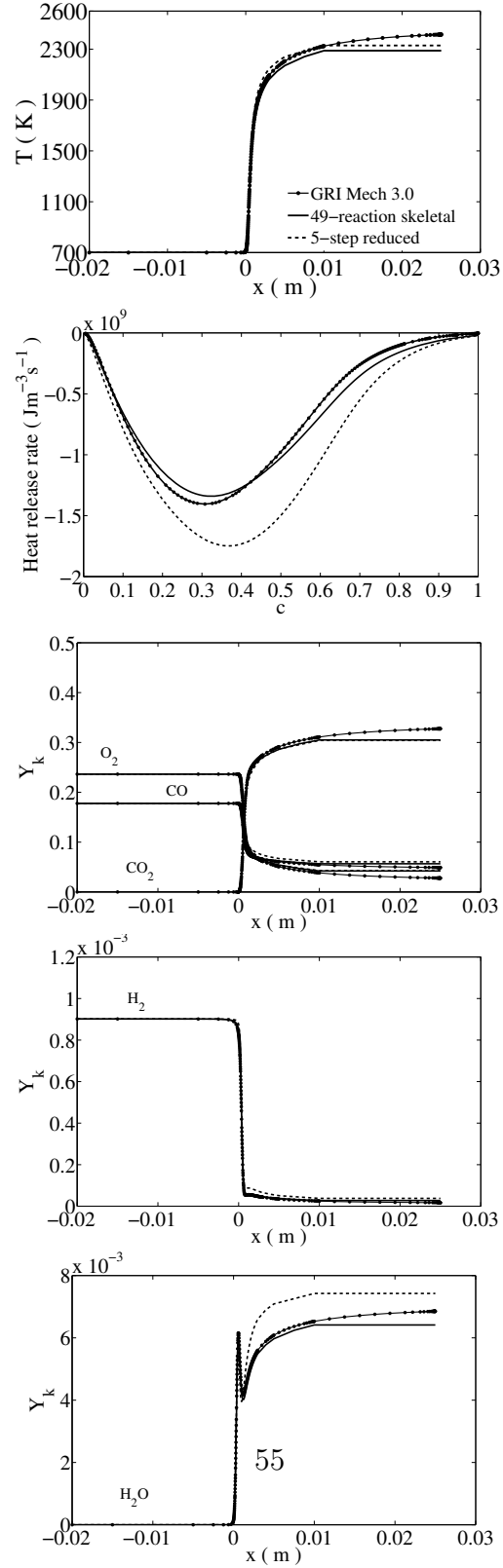
Fig. 16: Flame structure for $CO/H_2/O_2/N_2$. $\phi = 0.8$, $f_{H_2} = 5/95$, $T_u = 700$ K, $p = 1$ atm. (conditions as in Fig.5 top).

55
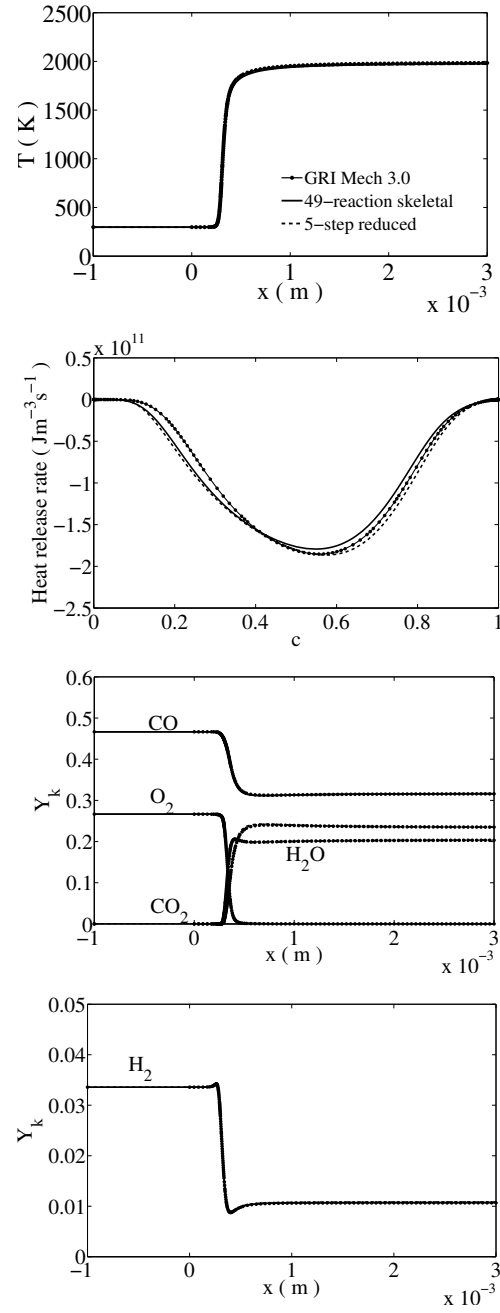
Fig. 17: Flame structure for $CO/H_2/O_2/He$. $He/O_2 = 7.0$, $\phi = 2.0$, $f_{H_2} = 1.0$, $T_u = 298$ K, $p = 5$ atm. (conditions as in Fig.8 top).
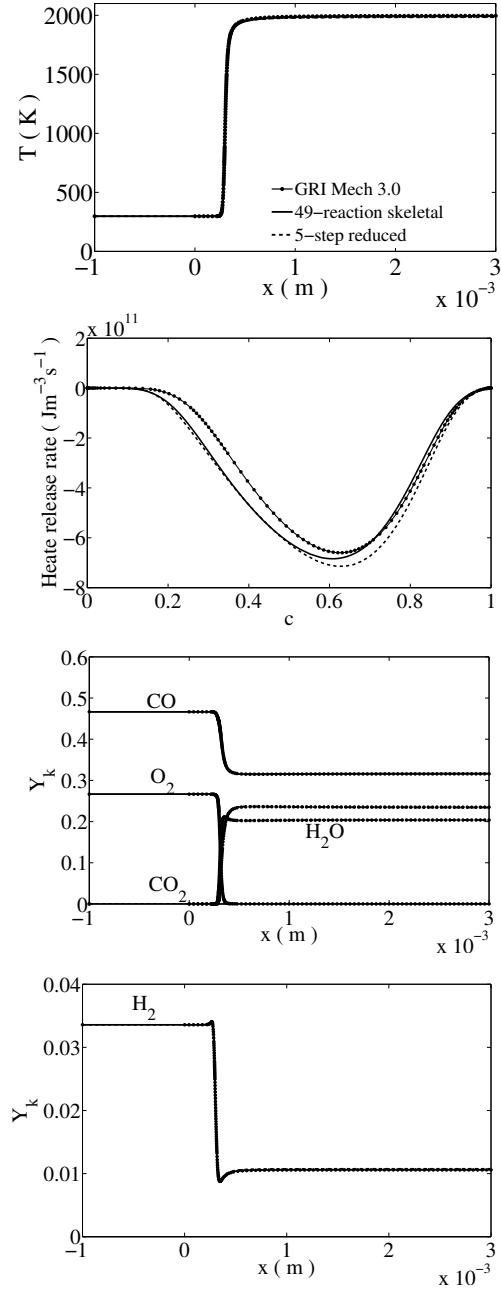
Fig. 18: Flame structure for $CO/H_2/O_2/He$. $He/O_2 = 7.0$, $\phi = 2.0$, $f_{H_2} = 1.0$, $T_u = 298$ K, $p = 10$ atm. (conditions as in Fig.8 top).

57
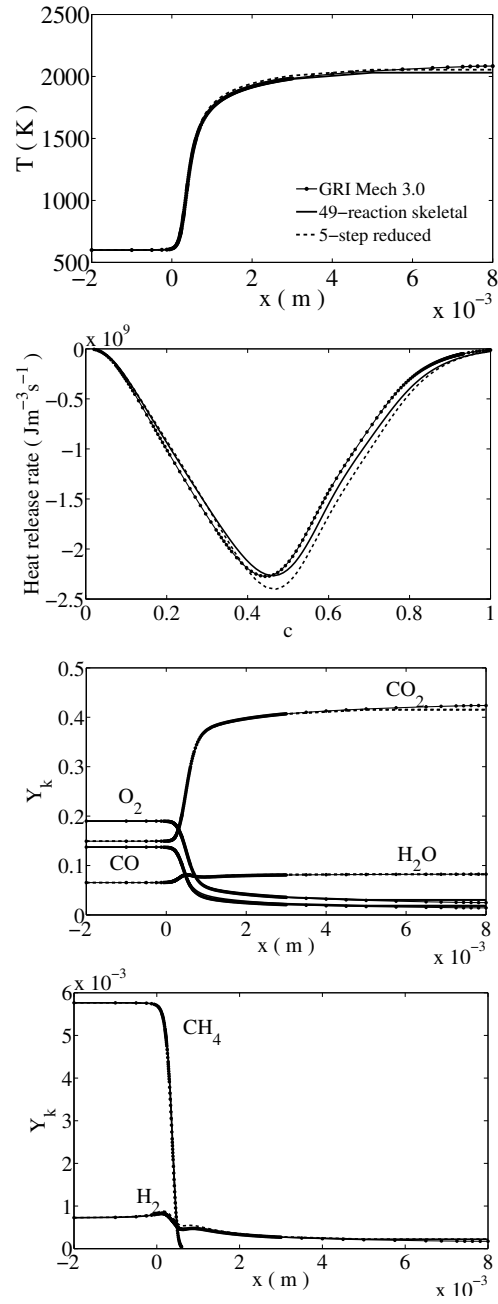
Fig. 19: Flame structure for $CO/H_2/CH_4/H_2O/CO_2/O_2/N_2$ with 25% H_2O. $\phi = 1.0$, $f_{H_2} = 5/95$, $f_{CH_4} = 5/95$, $f_{CO_2} = 0.5$, $T_u = 600$ K, $p = 1$ atm. (conditions as in Fig.11).

58
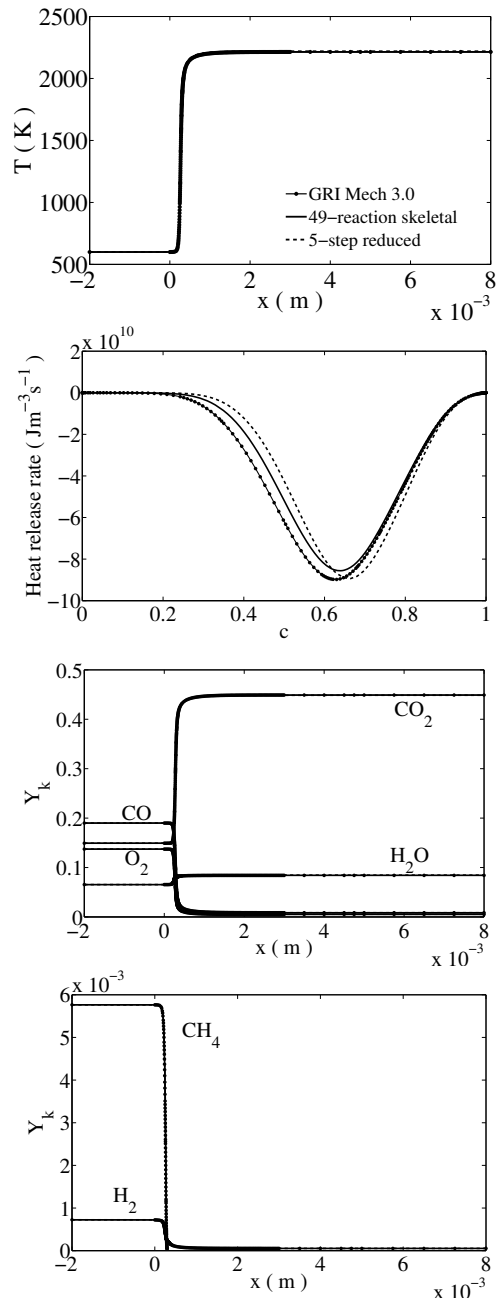
Fig. 20: Flame structure for $CO/H_2/CH_4/H_2O/CO_2/O_2/N_2$ with 25% H_2O. $\phi = 1.0$, $f_{H_2} = 5/95$, $f_{CH_4} = 5/95$, $f_{CO_2} = 0.5$, $T_u = 600$ K, $p = 10$ atm. (conditions as in Fig.11).

59
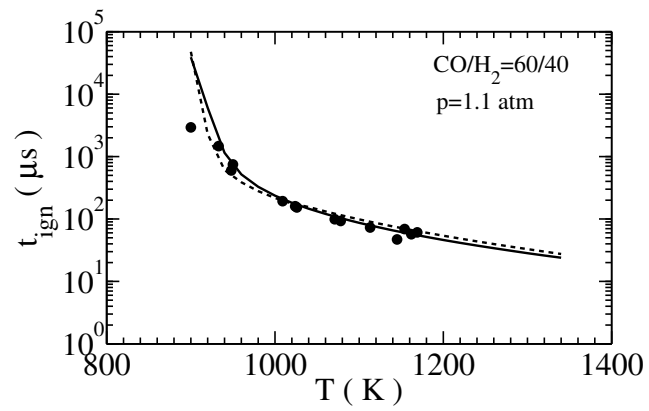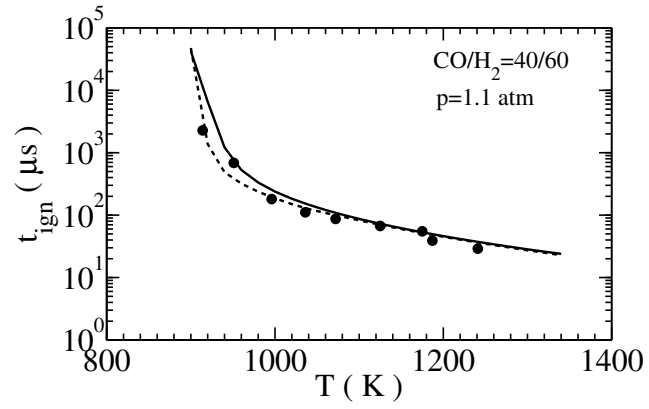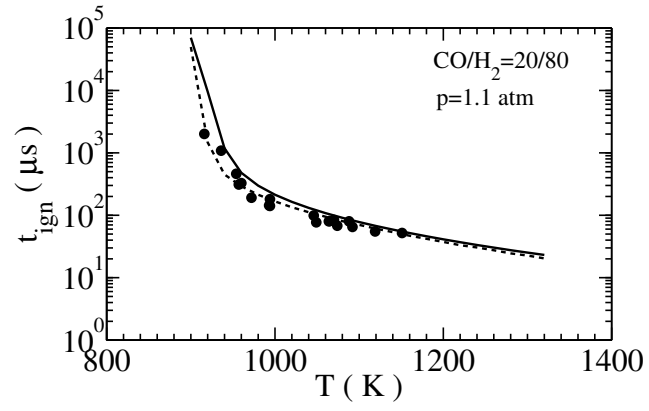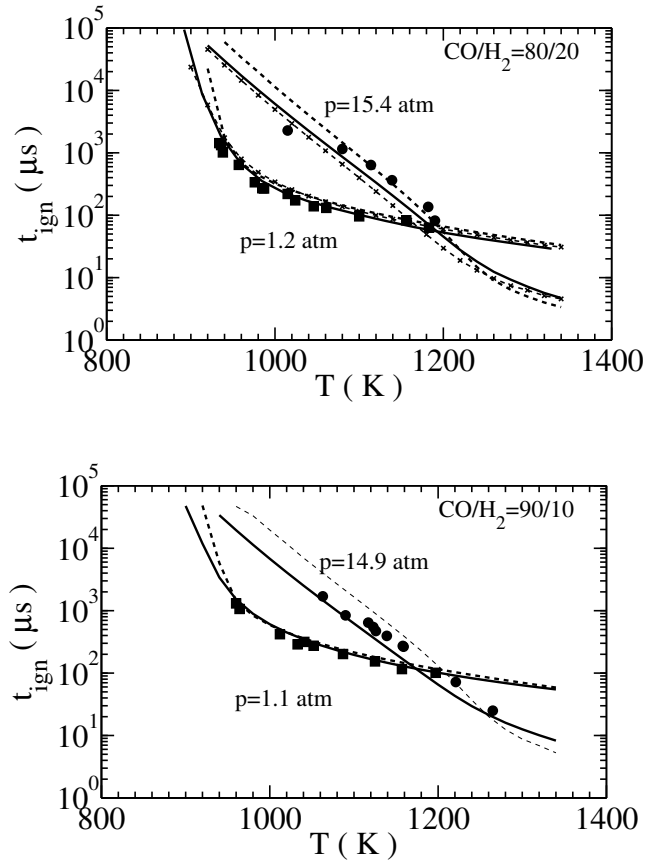
Fig. 21: Ignition delay times of $CO/H_2/O_2/N_2$ mixtures ($X_{N_2}/X_{O_2} = 3.76$) for $\phi = 0.5$ using the reduced (dashed lines) and skeletal (continuous lines) mechanisms. Symbols: experimental results of Kalitan et al. [55]. Also shown for comparison are the results with the skeletal mechanism of Boivin et al. [14] (dashed lines with ×) for the $f_{H_2} = 20/80$ case.
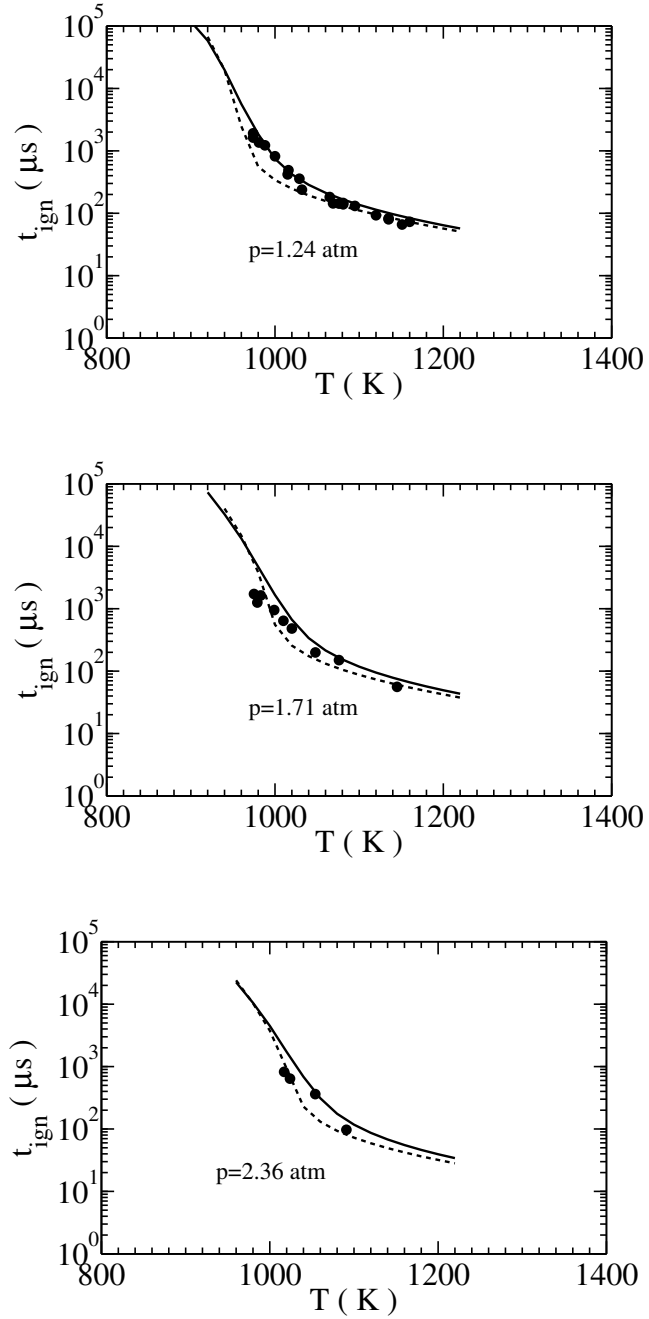
Fig. 22: Ignition delay times of $CO/H_2/CO_2/O_2/N_2$ mixtures using the reduced (dashed lines) and skeletal (continuous lines) mechanisms. Symbols: experimental data of [28], $8.91\%H_2 + 11.58\%CO + 24.44\%CO_2 + 10.25\%O_2 + 44.83\%N_2$.
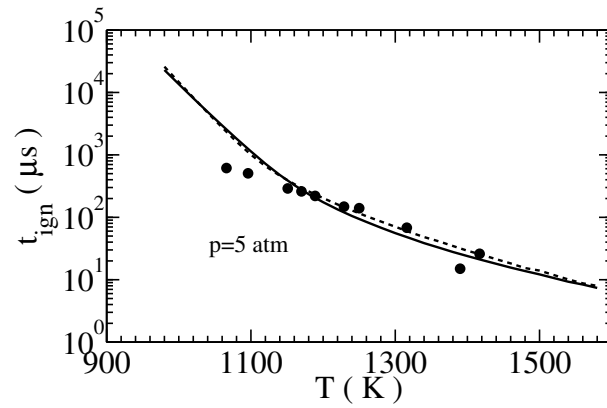
Fig. 23: Ignition delay times of $CO/H_2/H_2O/CH_4/O_2/N_2$ mixtures using the reduced (dashed lines) and skeletal (continuous lines) mechanisms. Symbols: experimental data of [56]. $\phi = 1$, $p = 5$ atm. Mixture: $3H_2 + CO + H_2O + 4O_2 + CH_4 + 16N_2$.

8. Appendix A

The range of conditions considered for the sensitivity analyses are given in Table A1. Two values for water content are considered. The raw sensitivity coefficients $k_i/s_l \partial s_l/\partial k_i$ are shown in Figs. A1 to A6 for $CO/H_2/H_2O$-air mixtures and in Figs. A7 to A12 for $CO/CH_4/H_2O$-air mixtures. If one were to conduct the sensitivity analyses for the ignition delays then the results would be very similar to those shown by Kalitan et al. [55] and thus they are not presented here.

p (atm)	T_u (K)	ϕ	f_{H_2}	f_{CH_4}	$H_2O\%$
1	323	0.9	5/95	0	0
1	323	0.9	5/95	0	20
1	323	0.9	1	0	0
1	323	0.9	1	0	20
1	323	2	5/95	0	0
1	323	2	5/95	0	20
10	600	0.9	5/95	0	0
10	600	0.9	5/95	0	20
10	1000	0.9	5/95	0	0
10	1000	0.9	5/95	0	20
20	600	0.9	5/95	0	20
1	323	0.9	0	5/95	0
1	323	0.9	0	5/95	20
1	298	0.9	0	1	0
1	323	0.9	0	1	20
1	323	2	0	5/95	0
1	323	2	0	5/95	20
10	600	0.9	0	5/95	0
10	600	0.9	0	5/95	20
10	1000	0.9	0	5/95	0
10	1000	0.9	0	5/95	20
20	600	0.9	0	5/95	20

Table A1: Conditions for sensitivity analysis.

8.1. Sensitivity analysis results

8.2. H$_2$-mixtures
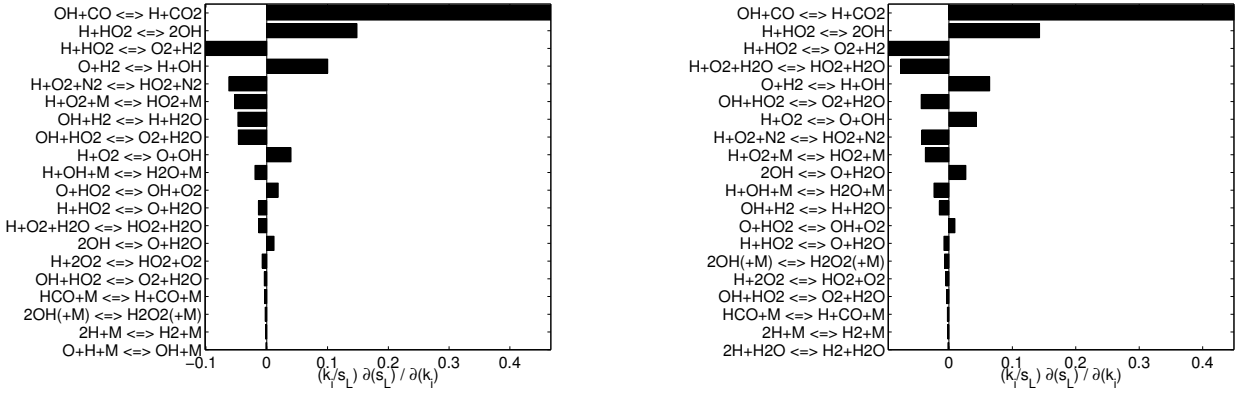
Fig. A 1: T_u=323 K, p=1 atm, ϕ=0.9, f_{H_2} = 5/95 with H$_2$O%=0 (left)%, 20(right)%
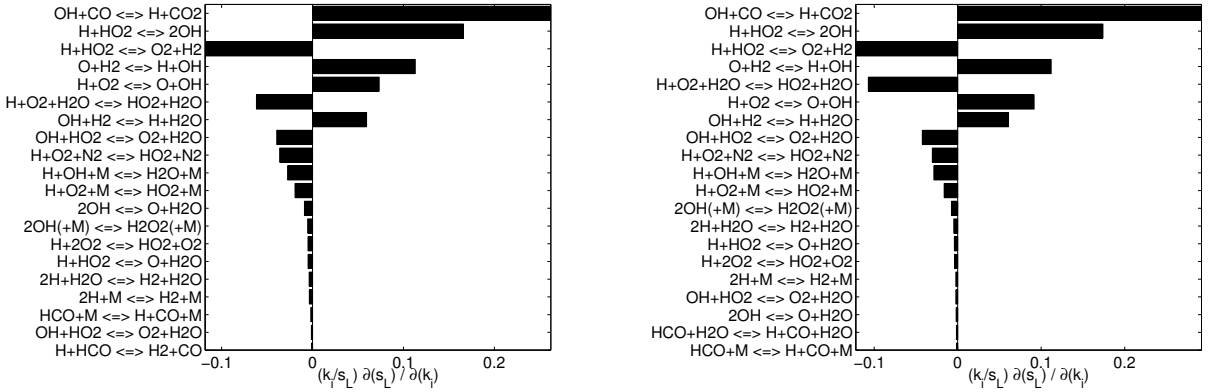
Fig. A 2: T_u=323 K, p=1 atm, ϕ=0.9, f_{H_2} = 1.0 with H$_2$O%=0 (left)%, 20(right)%
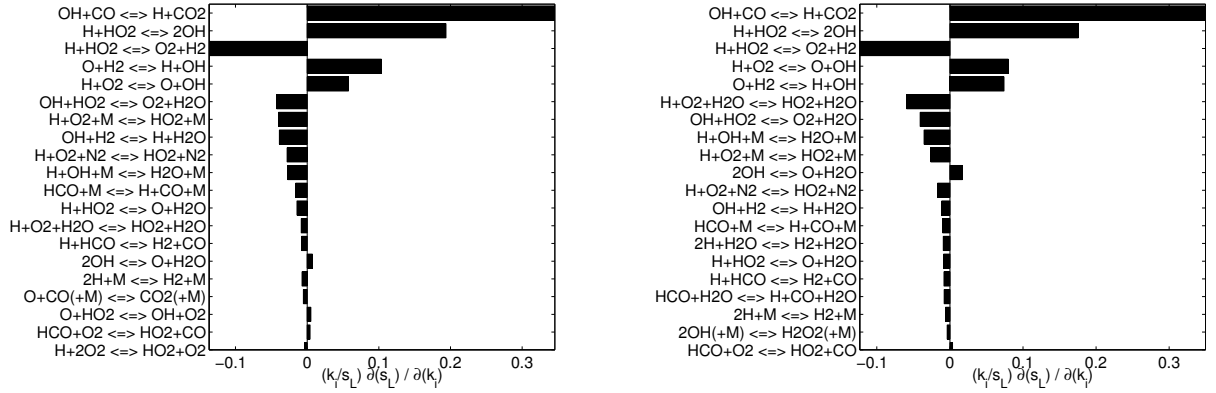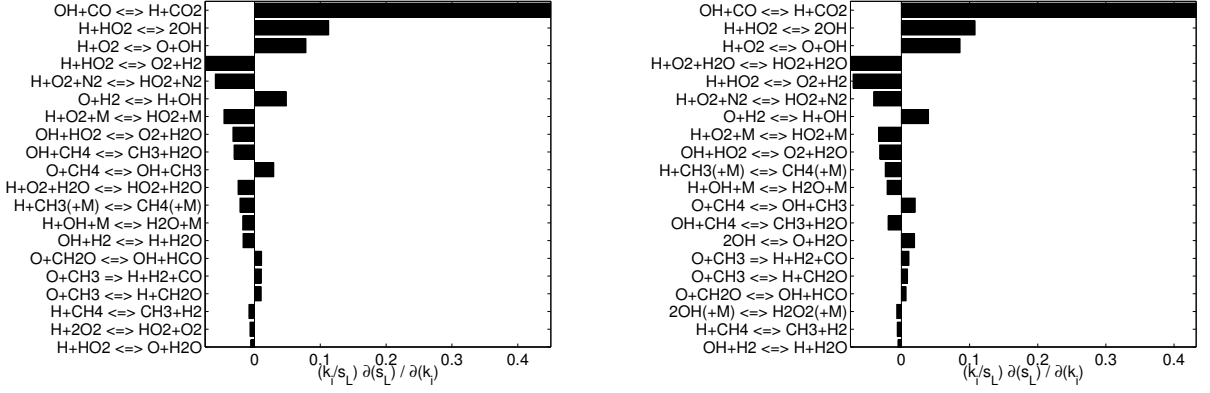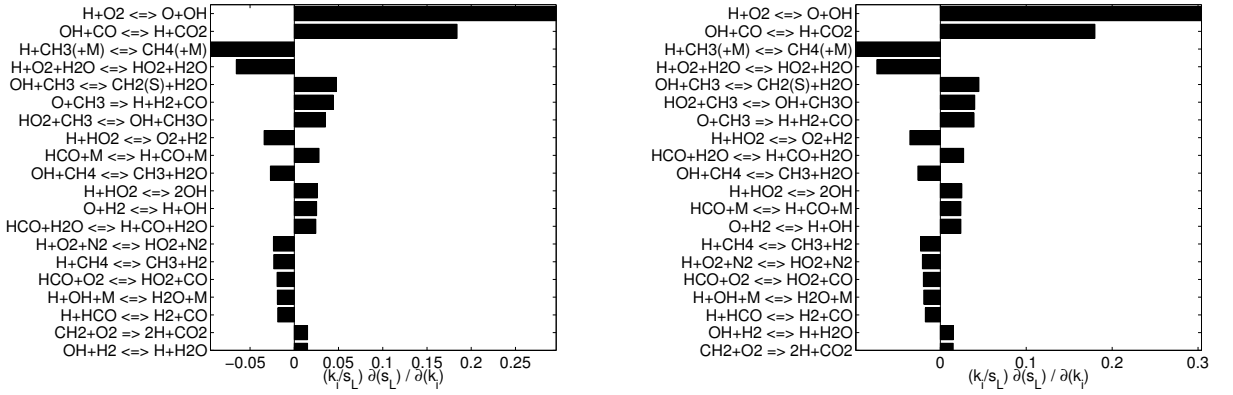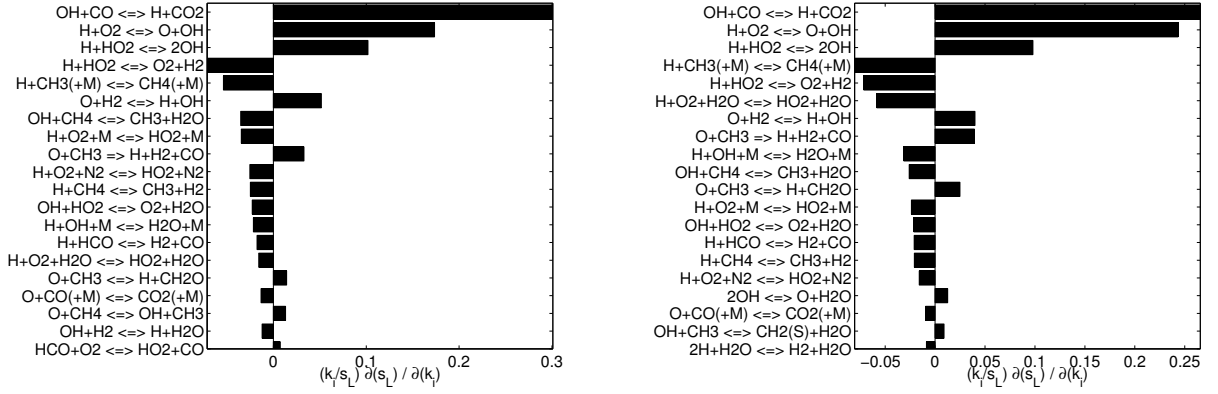
Fig. A 3: T_u=323 K, p=1 atm, ϕ=2.0, $f_{H_2} = 5/95$ with H2O%=0 (left)%, 20(right)%
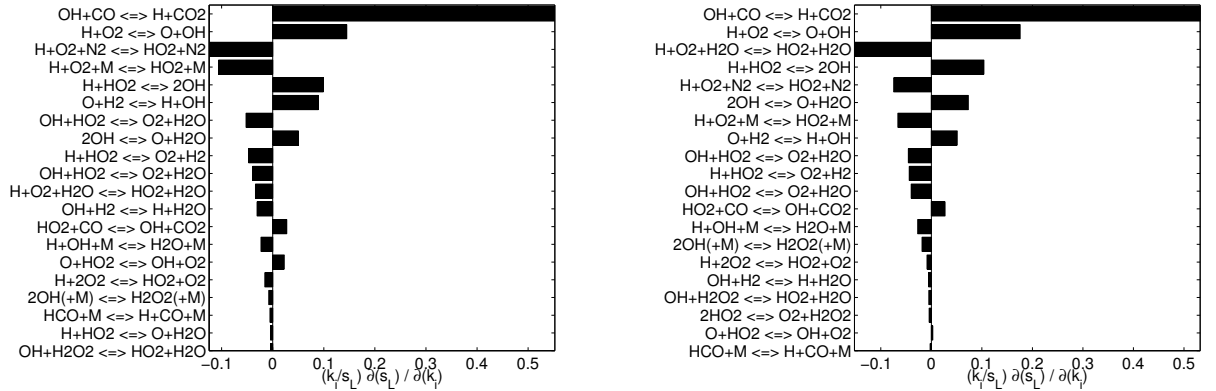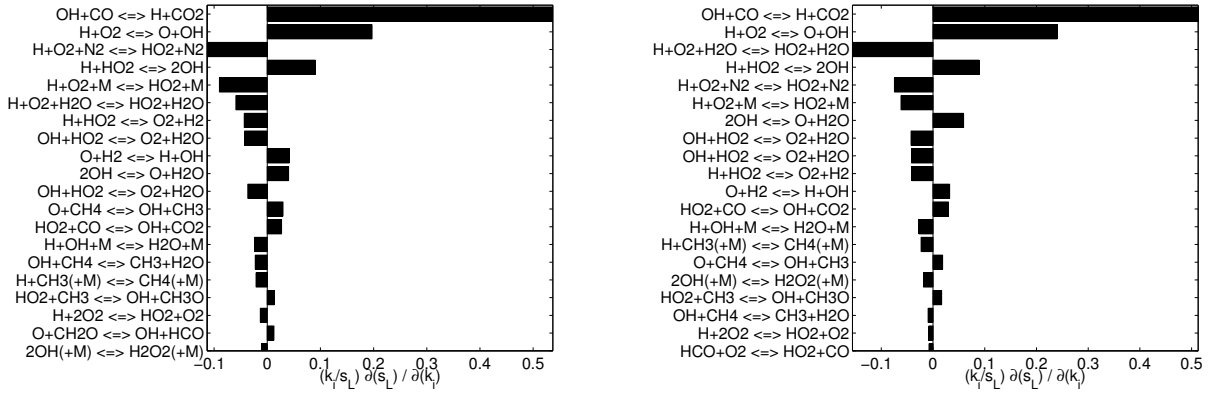

Fig. A 4: T_u=600 K, p=10 atm, ϕ=0.9, $f_{H_2} = 5/95$ with H2O%=0 (left)%, 20(right)%
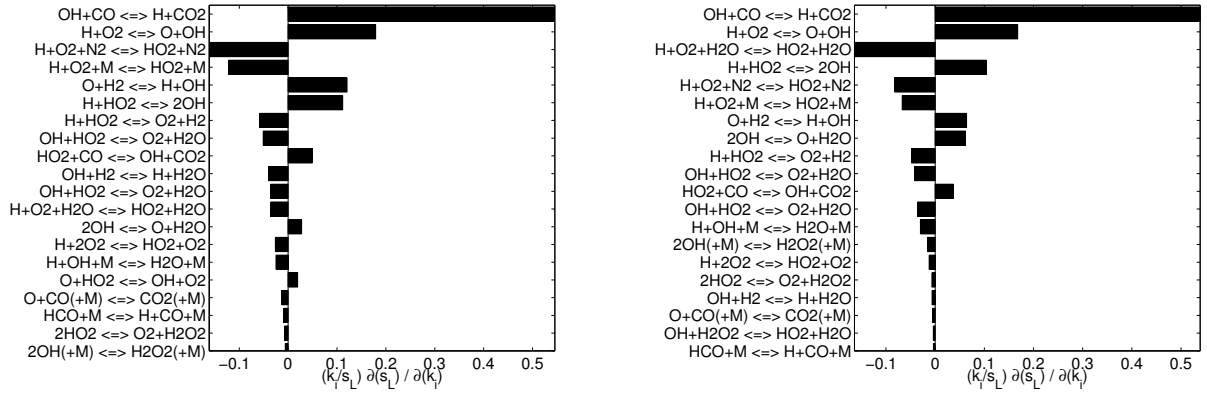
Fig. A 5: T_u=1000 K, p=10 atm, ϕ=0.9, $f_{H_2} = 5/95$ with H_2O%=0 (left)%, 20(right)%
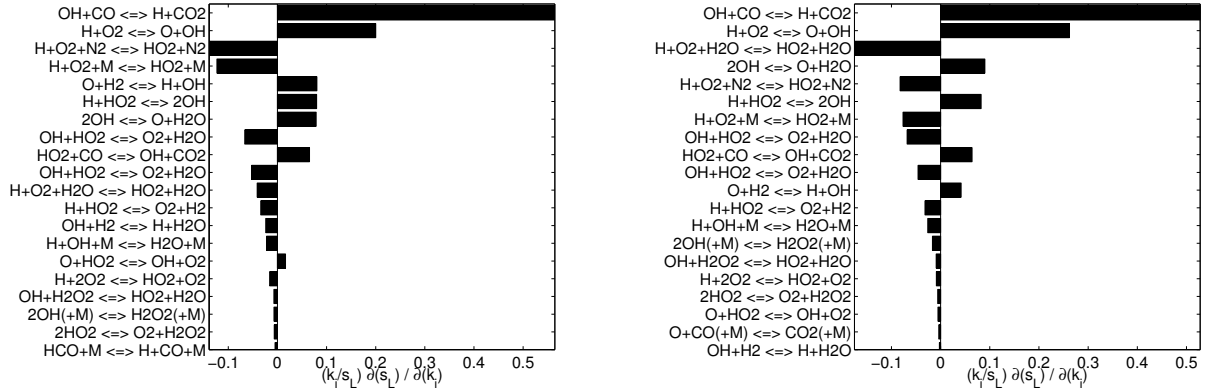
Fig. A 6: T_u=600 K, p=20 atm, ϕ=0.9, $f_{H_2} = 5/95$ with H_2O%=0 (left)%, 20(right)%

8.3. CH$_4$ mixtures

Fig. A 7: T_u=323 K, p=1 atm, ϕ=0.9, $f_{CH_4} = 5/95$ with H$_2$O%=0 (left)%, 20(right)%

Fig. A 8: T_u=323 K, p=1 atm, ϕ=0.9, $f_{CH_4} = 1.0$ with H$_2$O%=0 (left)%, 20(right)%

69

Fig. A 9: T_u=323 K, p=1 atm, ϕ=2.0, $f_{CH_4} = 5/95$ with H_2O%=0 (left)%, 20(right)%

Fig. A 10: T_u=600 K, p=10 atm, ϕ=0.9, $f_{CH_4} = 5/95$ with H_2O%=0 (left)%, 20(right)%
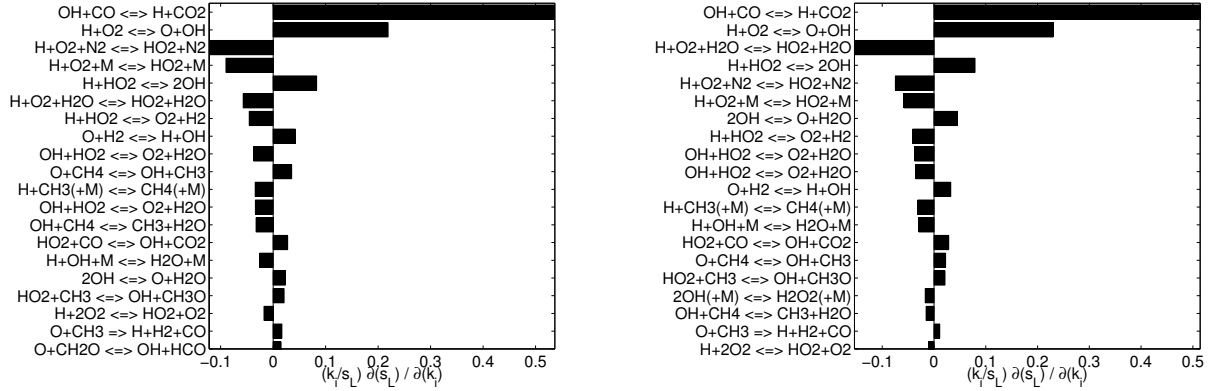
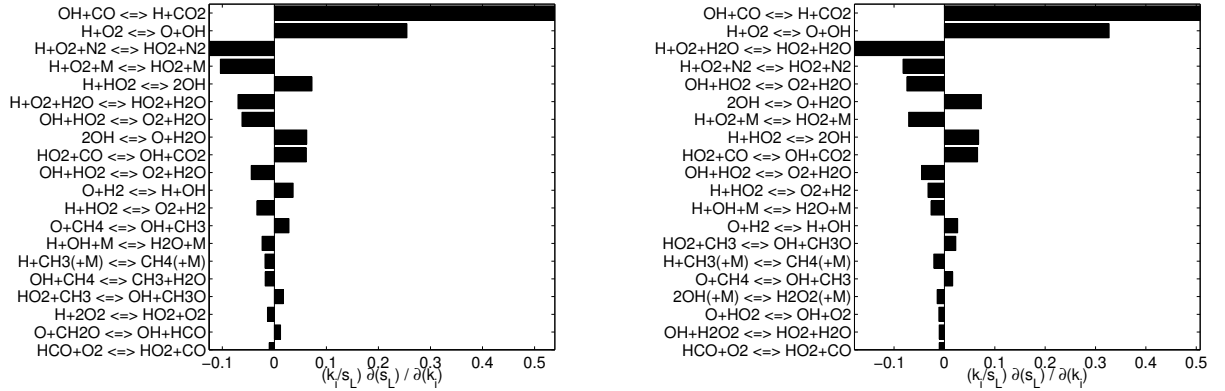Fig. A 11: T_u=1000 K, p=10 atm, ϕ=0.9, $f_{CH_4} = 5/95$ with H_2O%=0 (left)%, 20(right)%

Fig. A 12: T_u=600 K, p=20 atm, ϕ=0.9, $f_{CH_4} = 5/95$ with H_2O%=0 (left)%, 20(right)%

9. Appendix B

9.1. Non steady-state species rates

The global net reaction rate, $\dot{W}_k$, for species k involved in the 5-step reduced mechanism is given below. The numbers inside the bracket refer to the elementary reaction in the skeletal set in Table 3.

$\dot{W}_H=$
$-\dot{W}(1)+\dot{W}(2)+\dot{W}(3)-\dot{W}(5)-\dot{W}(6)-\dot{W}(7)-\dot{W}(8)-\dot{W}(9)-\dot{W}(10)-\dot{W}(11)-\dot{W}(12)-\dot{W}(15)-\dot{W}(20)-\dot{W}(23)-2\dot{W}(25)-2\dot{W}(26)-2\dot{W}(27)-2\dot{W}(28)-\dot{W}(29)-\dot{W}(31)+\dot{W}(32)-\dot{W}(35)+\dot{W}(38)+\dot{W}(39)+\dot{W}(40)+\dot{W}(43)+\dot{W}(44)-\dot{W}(46)-\dot{W}(47)-\dot{W}(48)$

$\dot{W}_{O_2}=$
$-\dot{W}(1)-\dot{W}(5)-\dot{W}(6)-\dot{W}(7)-\dot{W}(8)-\dot{W}(9)-\dot{W}(10)+\dot{W}(12)+\dot{W}(13)+\dot{W}(14)+\dot{W}(16)+\dot{W}(17)+\dot{W}(18)+\dot{W}(30)-\dot{W}(37)$

$\dot{W}_{H_2O}=$
$+\dot{W}(3)+\dot{W}(4)+\dot{W}(13)+\dot{W}(14)+\dot{W}(15)+\dot{W}(20)+\dot{W}(21)+\dot{W}(22)+\dot{W}(29)+\dot{W}(36)+\dot{W}(42)+\dot{W}(49)$

$\dot{W}_{CO}=$

$$-\dot{W}(32)-\dot{W}(33)-\dot{W}(34)+\dot{W}(35)+\dot{W}(36)+\dot{W}(37)+\dot{W}(38)+\dot{W}(39)+\dot{W}(44)$$

$\dot{W}_{CO_2}=$
$$\dot{W}(32)+\dot{W}(33)+\dot{W}(34)+\dot{W}(40)$$

$\dot{W}_{H_2}=$
$$-\dot{W}(2)-\dot{W}(3)+\dot{W}(12)+\dot{W}(23)+\dot{W}(25)+\dot{W}(26)+\dot{W}(27)+\dot{W}(28)+$$
$$\dot{W}(35)+\dot{W}(44)+\dot{W}(47)+\dot{W}(48)$$

$\dot{W}_{H_2O_2}=$
$$\dot{W}(17)+\dot{W}(18)+\dot{W}(19)-\dot{W}(20)-\dot{W}(21)-\dot{W}(22)-\dot{W}(23)-\dot{W}(24)$$

$\dot{W}_{CH_4}=$
$$-\dot{W}(41)-\dot{W}(42)+\dot{W}(46)-\dot{W}(47)$$

$\dot{W}_{N_2,He,Ar}=0$